Thermobarometry of meta-sedimentary enclaves in the Ten Mile Lake intrusion, Liscomb, Nova Scotia.

Helen McLaughlin

B.Sc. Honours Thesis
Department of Geology
Dalhousie University
April, 1990

Dalhousie University

Department of Geology
Halifax, Nova Scotia
Canada B3H 3J5
(902) 494-2358

DATE April 6, 1990

AUTHOR Helen Patricia McLaughlin

TITLE Thermobarometry of meta-sedimentary enclaves in the Ten Mile Lake intrusion, Liscomb, Nova Scotia.

Degree B.Sc. Convocation Spring Year 1990

Permission is herewith granted to Dalhousie University to circulate and to have copied for non-commercial purposes, at its discretion, the above title upon the request of individuals or institutions.

Distribution License

DalSpace requires agreement to this non-exclusive distribution license before your item can appear on DalSpace.

NON-EXCLUSIVE DISTRIBUTION LICENSE

You (the author(s) or copyright owner) grant to Dalhousie University the non-exclusive right to reproduce and distribute your submission worldwide in any medium.

You agree that Dalhousie University may, without changing the content, reformat the submission for the purpose of preservation.

You also agree that Dalhousie University may keep more than one copy of this submission for purposes of security, back-up and preservation.

You agree that the submission is your original work, and that you have the right to grant the rights contained in this license. You also agree that your submission does not, to the best of your knowledge, infringe upon anyone's copyright.

If the submission contains material for which you do not hold copyright, you agree that you have obtained the unrestricted permission of the copyright owner to grant Dalhousie University the rights required by this license, and that such third-party owned material is clearly identified and acknowledged within the text or content of the submission.

If the submission is based upon work that has been sponsored or supported by an agency or organization other than Dalhousie University, you assert that you have fulfilled any right of review or other obligations required by such contract or agreement.

Dalhousie University will clearly identify your name(s) as the author(s) or owner(s) of the submission, and will not make any alteration to the content of the files that you have submitted.

If you have questions regarding this license please contact the repository manager at dalspace@dal.ca.

Grant the distribution license by signing and dating below.

_____ _____

Name of signatory Date

TABLE OF CONTENTS

List of Figures

List of Tables

Abstract

A section of a drill core from the area of the Ten Mile Lake, Liscomb Complex, Nova Scotia, contains many small metasedimentary enclaves in a felsic host. The enclaves investigated are calc-silicate and metapelites and range from having distinct to gradational boundaries and from to being intact to extremely disaggregated within the host.

The enclaves contain both xenoblastic, pre-magma entrainment and idioblastic, syn-magma entrainment minerals. Relict phases in the metapelites are Mn-rich and Mn-poor xenoblastic garnets, kyanite, sillimanite, biotite, plagioclase, zincian hercynite, and staurolite. Syn-entrainment mineral assemblage includes Mn-rich and Mn-poor idioblastic garnets, fibrolite, biotite, plagioclase, and muscovite. Other phases include quartz, sphene, pyrite, chalcopyrite, Fe-Ti oxides, and retrograde chlorite. Calc-silicate enclaves contain grossular, dolomite, zoisite, clinozoisite, epidote, hornblende, apatite, sphene, quartz, plagioclase, pyrite, and chalcopyrite.

Zincian hercynite, present in the source region, reacted to form staurolite during coupled retrograde and metasomatic metasomatic reactions. Zonation of garnets and the calc-silicate enclaves and carbonate and quartz veinlets are further evidence for chemical exchange between the enclaves and the host. The source region for the enclaves is determined to be pelitic and calc-silicate, locally rich in zinc.

Pressure and temperatures are determined for pelitic enclaves in a tonalite to quartz-diorite intrusion in the Ten Mile Lake gabbro area are based on garnet-biotite-plagioclase - Al_2SiO_5-quartz geothermobarometry in the pelitic enclaves. Temperature and pressures for pre-entrainment metamorphism of the enclaves are 780 ± 50 °C and 5.6 ± 1.5 kb. Syn-entrainment metamorphism is estimated at 560 ± 50 °C and 2.3 ± 1.5 kb.

Petrography shows that pre-entrainment P-T estimates may not be coincident, but rather may represent independent maximums. Mineralogy suggests that the source region, at ~ 17 km, was initially at lower temperatures than indicated by thermometry calculations. The initial intrusion of the magma led to an increased temperature, at a maximum of ~ 780 °C, before entrainment into the magma.

CHAPTER 1: INTRODUCTION

1.1 Enclaves in Igneous Rocks

Study of the lower crust is possible as a result of the incorporation of enclaves into a magma. Hot magma ascends through crust and injects into pre-existing planes of weakness, seeping into fractures defined by bedding planes or secondary structures in the country rock. The fractures propagate through the host rock, eventually separating small fragments to large sections, up to a kilometer in size, from the wall rock. These may become entirely enveloped by the magma. The melt consumes the host rock fragments by chemical exchange between the melt and the enclaves and by physical disaggregation of the material through mechanical breakdown. Rapid ascent to the upper crust limits the chemical and physical degradation of the enclaves.

Occurrence of crustal xenoliths in a magma involves the incorporation of crustal material in the melt and subsequent rapid ascent allowing preservation of the crustal fragments. Relict, pre-entrainment pressure and temperature conditions may also be preserved. Lower crustal xenoliths allow the material at depth to be studied. Enclaves in the Ten Mile Lake area, and the implications they have on our understanding of the material which underlies the Meguma Group, have been examined in this light. The Ten Mile Lake gabbro of the Liscomb Complex is attributed to the rapid ascent of the Liscomb gabbros to a volatile-rich magma (Giles and Chatterjee 1987a; 1986). Core from a drill hole in an intrusion in the Ten Mile Lake area in the vicinity of its contact with the high-grade gneisses of the Liscomb Complex is the source of samples for this study. The samples are from a 1.24 meter section in the upper portion of the core. The core contains many small (up to 4 cm) pelitic and calc-silicate enclaves in a felsic matrix.

1.2 The Approach

1.2.1 Nature of the Problem

This is a study of metamorphism observed in enclaves in the Ten Mile Lake gabbro, and of their possible origin. Metamorphic assemblages, reactions, mineralogy, and textural relationships provide constraints for metamorphic facies determination. Temperature and depth estimates of the protolith regional metamorphism and and subsequent pluton emplacement are determined through petrology and thermobarometry.

1.2.2 Purposes of the Study

1) Mineral identification including mineral chemistry, zonation, texture, size, and reactions; and further classification of minerals based on their association with pre-entrainment or syn-entrainment metamorphism.

2) Determination of the temperature conditions during metamorphism using garnet-biotite geothermometry with microprobe analyses of coexisting equilibrium garnet and biotite.

3) Determination of the maximum pressure conditions of metamorphism using garnet-plagioclase-Al_2SiO_5-quartz geobarometry with microprobe analyses of coexisting garnet and plagioclase in equilibrium with Al_2SiO_5 and quartz.

4) Attempt to determine the origin of the enclaves as belonging to the Meguma Group, Liscomb gneisses, or another source based on comparison of mineral assemblage, inferred bulk chemistry, and P-T conditions of these and other rocks.

1.2.3 Scope of the Study

This investigation is limited to twenty-four xenoliths (nineteen pelitic, two pelitic and calc-silicate hybrids, two pelitic and quartz hybrids, and one calc-silicate) from a 1.24 meter section of the drill core. Petrographic observations and microprobe analyses of minerals are used to determine the P-T conditions of the metamorphism. Whole-rock chemical analyses were not done on either enclaves or the intrusion. This thesis deals only with the pressure and temperature conditions of metamorphism in the enclaves, and possible origin based on mineral assemblages.

1.2.4 Organization of the Thesis

The thesis begins with a classification of the enclaves on the basis of mineral assemblage, and attempts to determine the possible source or sources of the enclaves present using mineral assemblage, mineral chemistry, and P-T conditions. Conditions of metamorphism are determined on the basis of mineral assemblage, texture and reactions. Mineral chemistry, obtained from microprobe analyses, and garnet - biotite - plagioclase - Al_2SiO_5 - quartz thermobarometry are used to determine estimates of the conditions of metamorphism. An interpretation of the data, construction of a pressure - temperature path (P-T path), and implications for the origin of the enclaves are discussed.

CHAPTER 2: GEOLOGICAL SETTING

2.1 Regional Geology

The Liscomb Complex is located in central Nova Scotia (Fig. 2.1). The Cambrian - Ordovician Meguma Group, consisting of the Halifax Formation slates and Goldenville Formation quartzites, was deformed into northeast - southwest trending folds during the Acadian Orogeny (415 - 400 Ma) (Fig. 2.1).

Figure 2.2 shows the metamorphic facies and zones of the Meguma Group in central Nova Scotia as summarized by Douma (1988). In the central part of the Meguma Terrane, including the study area, regional metamorphic grade does not exceed the greenschist facies (chlorite zone). Mineralogy includes quartz, relict detrital feldspar, muscovite, chlorite, $\pm$ Fe-Ti oxides, tourmaline, rutile, and rare biotite. The Meguma terrane east and south of the main Liscomb Complex and east, west, and north of the Ten Mile Lake gabbro is metamorphosed to the biotite zone of the greenschist facies with a characteristic mineral assemblage of quartz, clastic feldspar, muscovite, chlorite, biotite, $\pm$ tourmaline, Fe-Ti oxides, and epidote.

The Meguma Group reaches the amphibolite facies near a granitic complex in the Crow's Nest area. The mineral assemblage of this lower amphibolite facies Meguma Group includes quartz, feldspar, biotite, muscovite, Fe-Ti oxides, $\pm$ staurolite, cordierite, garnet, tourmaline, and retrograde chlorite. In the most southwestern area of Nova Scotia, the Meguma Group reaches upper amphibolite facies. The mineral assemblage is characteristically andalusite, biotite, cordierite, staurolite, garnet with minor sillimanite.

Late Devonian (370 Ma) gabbroic rocks, granitoids, gneisses and schists of the Liscomb Complex intrude the Meguma Group metasediments (Giles and Chatterjee 1987a; 1986) in central Nova Scotia (Fig 2.3); the complex is separated

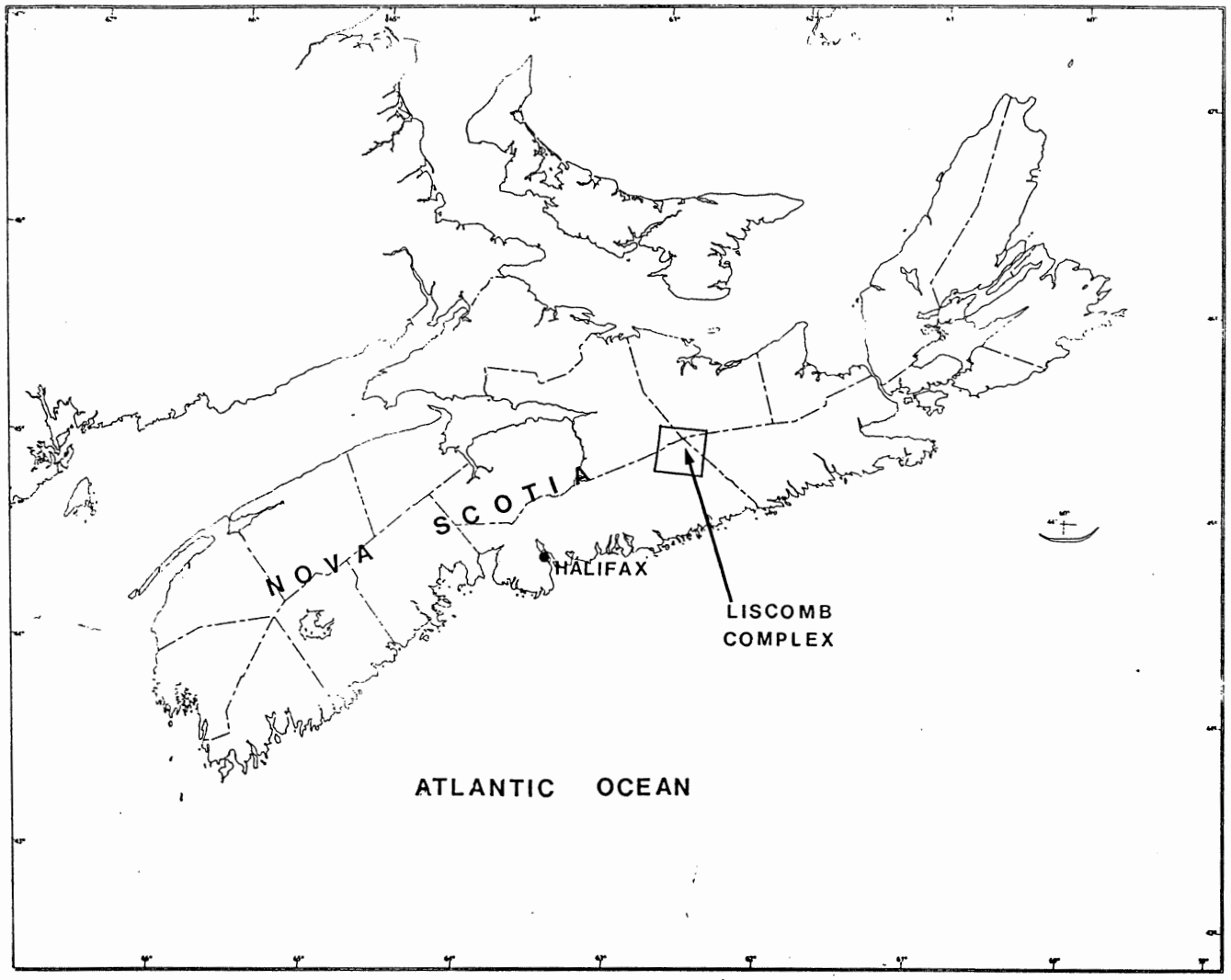

Figure 2.1. Regional Location Map.

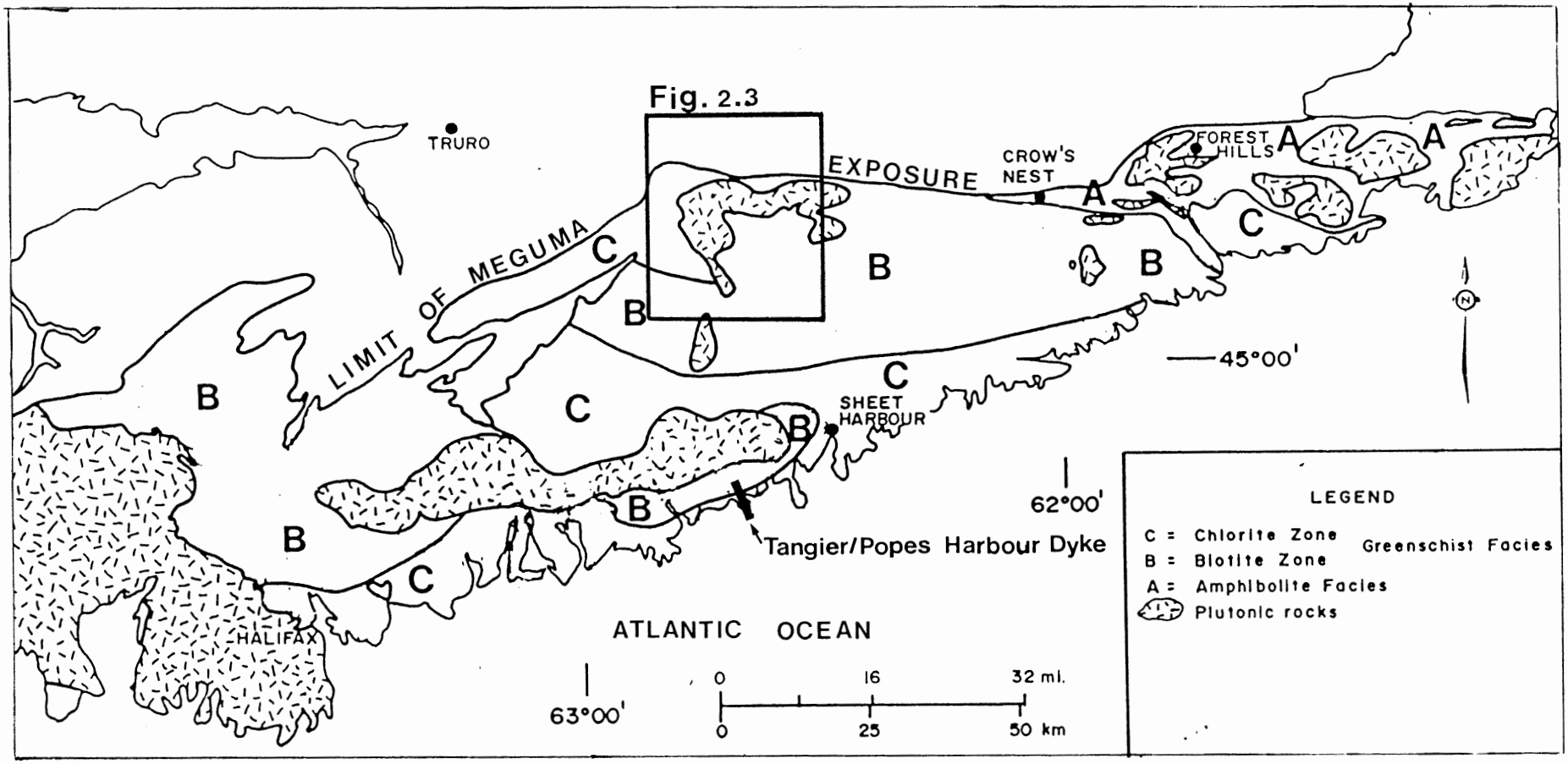

Figure 2.2. Metamorphic Zones and Facies of the Meguma Terrane in Central Nova Scotia (after Keppie and Muecke 1979).

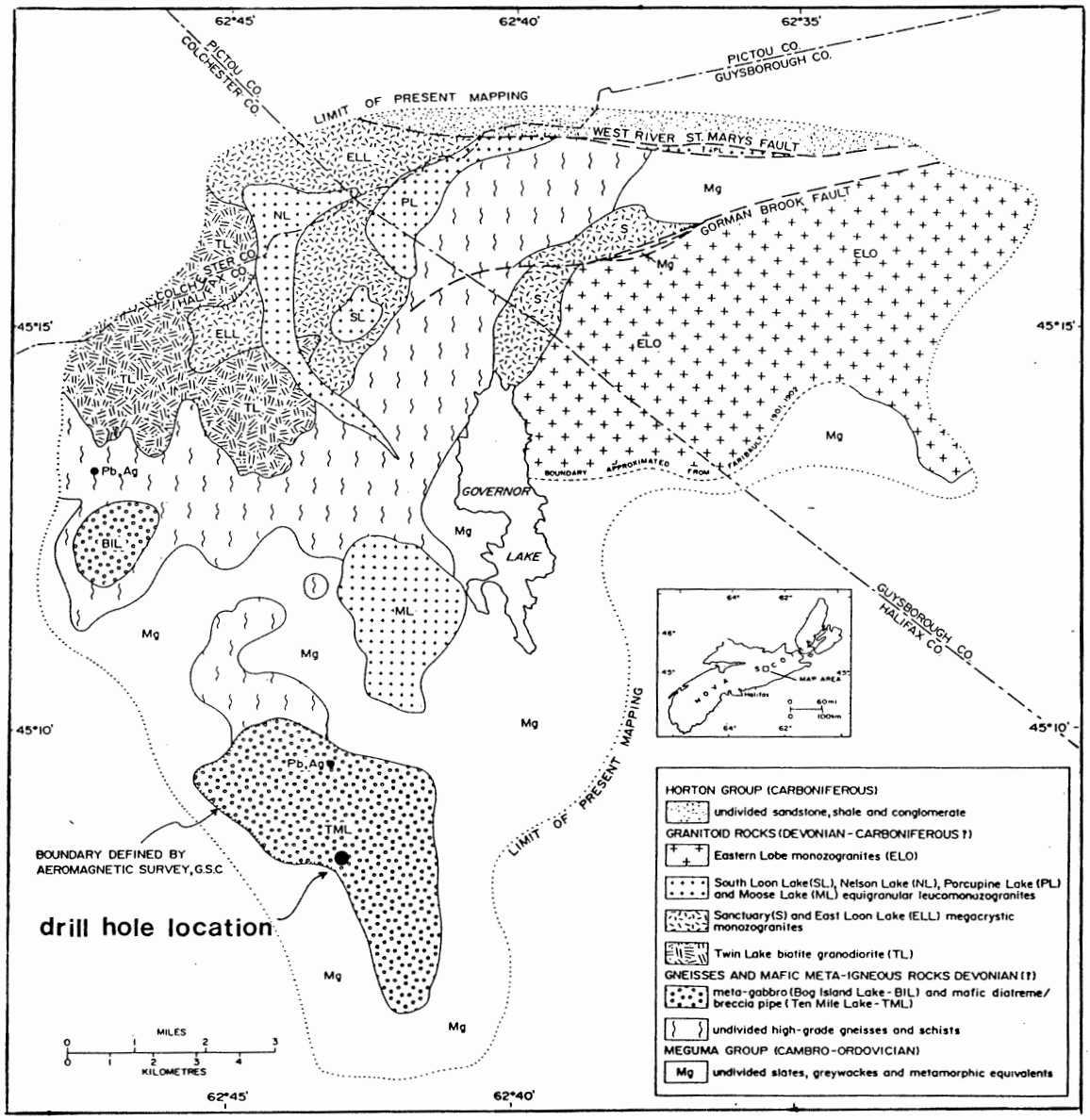

Figure 2.3. Location Map (after Giles and Chatterjee 1986).

from the Carboniferous Horton Group sandstone, shales, and conglomerates to the north by the West River-St Mary's Fault.

2.2 The Liscomb Complex

The Liscomb intrusion, covering 350 km^2, was first mapped by Faribault (1901, 1902) as a single pluton. Recently, detailed mapping of gabbro, gneisses and granites led to the separation of the intrusion and its name, the Liscomb Complex (Giles and Chatterjee 1986). The entire complex consists of two gabbro plutons, eight peraluminous granitic plutons, and high-grade gneisses and schists.

The Ten Mile Lake and Bog Island Lake gabbros and diorites intrude the Meguma and the Liscomb gneisses. The mafic plutons range in composition from quartz - gabbro to quartz - diorite and contain abundant enclaves (Giles and Chatterjee 1987a).

The granitic plutons are further divided into one fine- to coarse - grained muscovite - biotite monzogranite, four equigranular muscovite - biotite monzogranites, two megacrystic biotite monzogranites, and one biotite granodiorite (Giles and Chatterjee 1987a; 1986) (Fig. 2.3). These include the Eastern Lobe monzogranites, South Loon Lake, Nelson Lake, Porcupine Lake, and Moose Lake equigranular leucomonzogranites, Sanctuary and East Loon Lake megacrystic monzogranites, and Twin Lake biotite granodiorite (Giles and Chatterjee 1987a; 1986).

The high-grade gneisses and schists, enveloping the plutons, contain a foliation that trends obliquely to the NE - SW striking folds of the Meguma Group. Mineralogy includes orthopyroxene, clinopyroxene, garnet, hornblende, and Al-silicates. Also, they are chemically distinct from the Meguma Group (Giles and Chatterjee 1987a).

Giles and Chatterjee (1987a) suggested a mixed volcanic - sedimentary

protolith for the high grade gneisses and schists, and inferred that they diapirically intrude the older, geochemically different Meguma Group. Field relations suggest that emplacement of the mafic plutons, the metamorphic suite, and the granite post - dated the Meguma Group deformation. New data (Chatterjee, *unpubl. pers. comm. 1989*) indicates that the mafic intrusions are slightly older (~ 375 Ma) than the gneisses and granites (~ 370 Ma), consistent with the field relations.

2.3 Sample Location

Figure 2.3 illustrates the location of a hole drilled by the Nova Scotia Department of Mines and Energy (NSDME) in an intrusive in the Ten Mile Lake area at its contact with the Liscomb gneisses. The hole is located at latitude and longitude 45° 07' 37" and 62° 41' 56". The core penetrates a felsic host which contains many small pelitic and calc-silicate enclaves of amphibolite facies.

These enclaves are significant in understanding the composition and structure of the lower crust and determining the depth of the host intrusion.

2.4 Enclaves in the Tangier/Popes Harbour Dyke Along Eastern Shore, Nova Scotia

The Tangier/Popes Harbour dyke is a mafic unit located south of the Liscomb Complex, along the eastern shore of Nova Scotia (Fig. 2.3). Xenoliths within this dyke are interpreted as fragments of the lower crust. The proximity to the Liscomb Complex and its similar mafic composition may indicate that enclaves in the Ten Mile Lake intrusion and the Tangier/Popes Harbour dyke are of similar origin. The enclaves in the Tangier/Popes Harbour dyke are compared with the Ten Mile Lake enclaves on the basis of mineralogy and depth of origin.

Owen *et al.* (1988) describe gneissic pelitic and tonalitic xenoliths in a mafic dyke at Popes Harbour. The pelitic xenoliths contain sillimanite, kyanite (relict), kyanite pseudomorphs of sillimanite, biotite, pyrope, brown spinel (X_{Mg} = 0.45-0.65), red sapphirine, corundum, rutile, oligoclase - andesine, ternary feldspar,

Fe-Ti oxides, minor quartz and local chlorite. The tonalitic xenoliths contain almandine, ferrohypersthene, andesine, quartz, biotite, amphibole, and minor chlorite. Pressures of 4.5 - 6 kb and temperatures greater than 600 °C are given for pre-entrainment metamorphism. No estimates for syn-entrainment metamorphism are given.

Eberz *et al.* (1989), Chatterjee and Giles (1988), Eberz *et al.* (1988), and Giles and Chatterjee (1987) discuss sedimentary and igneous granulite facies xenoliths in the Tangier Dyke. The metasedimentary xenoliths contain garnet, quartz, biotite, alkali feldspar, minor plagioclase, mesoperthite, graphite, corundum, rutile, chlorite, muscovite, $\pm$ sapphirine, orthopyroxene, clinopyroxene, amphibole, spinel, kyanite, sillimanite, epidote and sphene. Meta-igneous xenoliths contain clinopyroxene, amphibole, quartz, biotite, alkali feldspar, labradorite, phlogopite, calcite, chlorite, sphene, epidote $\pm$ orthopyroxene. Peak pressure and temperature estimates for pre-entrainment metamorphism are placed at 12-14 kb and greater than 1000 °C.

CHAPTER 3: PETROGRAPHY AND MINERAL CHEMISTRY

3.1 Hand Sample Description

The core contains many small mafic and calc-silicate enclaves in a felsic host. The mafic enclaves, up to 4 - 5 cm, are rounded to angular and may appear as distinct foreign material in the host or, commonly, as ghost enclaves in a felsic matrix. They range in composition from biotite- to garnet-rich. The calc-silicate enclaves are commonly rounded rather than angular and are similar in size to the mafic enclaves. They commonly show zoning from the core to their contact with the host which may be either sharp to gradational. Where the contact is distinct, the calc-silicate enclave is rimmed with quartz and has a core of garnet and epidote and veinlets penetrating into the host. Aluminum silicate and biotite wisps are common in the felsic matrix.

The mineralogy of the mesocratic, fine-grained, host includes quartz, biotite, oligioclase-andesine, muscovite, Fe-Ti oxides, pyrite, chalcopyrite, and tourmaline. The host is roughly tonalite to quartz - diorite in composition and contains no amphibole or pyroxene. In contrast, the Ten Mile Lake host is described by Richard (*manu. in prep.*) as containing quartz, plagioclase, amphibole, biotite, and muscovite and are compositionally quartz - gabbro to quartz - diorite. Gabbroic enclaves in the Ten Mile Lake mafic intrusion (samples LG-139, LG-162, and LG-165) contain quartz, plagioclase, clinopyroxene, amphibole, biotite, chlorite, and muscovite (Richard, *manu. in prep.*).

The Ten Mile Lake mafic intrusion gives pressures of 3.3 $\pm$ 1 kb, indicative of syn-entrainment conditions. Its gabbroic enclaves give pressures of 5.2 $\pm$ 1 kb is indicative of pre-entrainment conditions. Both are based on hornblende geobarometry (Richard, *manu. in prep.*).

Thus, the core from this study appears to have penetrated an intrusion different in composition from the quartz-gabbro and quartz-diorite described by (Giles and Chatterjee 1987a; 1987b). This is most apparent with the lack of amphibole in this intrusion compared to its presence in the mafic intrusions described by Richard (*manu. in prep.*) previous studies of the Ten Mile Lake gabbro and its enclaves.

3.2 Petrography of the Enclaves

Meta-sedimentary enclaves from the Ten Mile Lake gabbro include nineteen pelites, two hybrid pelites with calc-silicate nodules, two hybrid pelites with a quartz inclusion, and one calc-silicate. The pelitic enclaves characteristically contain biotite, garnet, quartz, fibrolite, muscovite, plagioclase, chlorite, sphene, Fe-Ti oxides, pyrite, and chalcopyrite, with minor spinel, staurolite, apatite, sillimanite, and kyanite. In discussion of the aluminum silicates in this text, the term 'sillimanite' is restricted to the coarse variety, and 'fibrolite' to the fibrous variety of sillimanite. Mineralogy specific to each enclave may be found in Appendix I and description of textures in Appendix II. All photographs show plane polarized light (PPL) with the exception of Figures 3.14 and 3.15 which show crossed nicols (XN).

Pelites. The enclaves from the Ten Mile Lake gabbro show compositional variation reflected in mineral assemblages of individual enclaves. Figure 3.1 shows an angular garnet- and biotite-rich inclusion and a slightly rounded biotite-rich inclusion in a quartz- and plagioclase-rich felsic host. The mafic enclaves are generally rich in biotite and plagioclase, and may contain small idioblastic garnets. Figure 3.2 shows sillimanite- and biotite-rich schlieren in a sillimanite- and biotite-poor matrix. Figure 3.3 illustrates mineralogical and chemical zonation with layers rich in biotite and small idioblastic garnets within

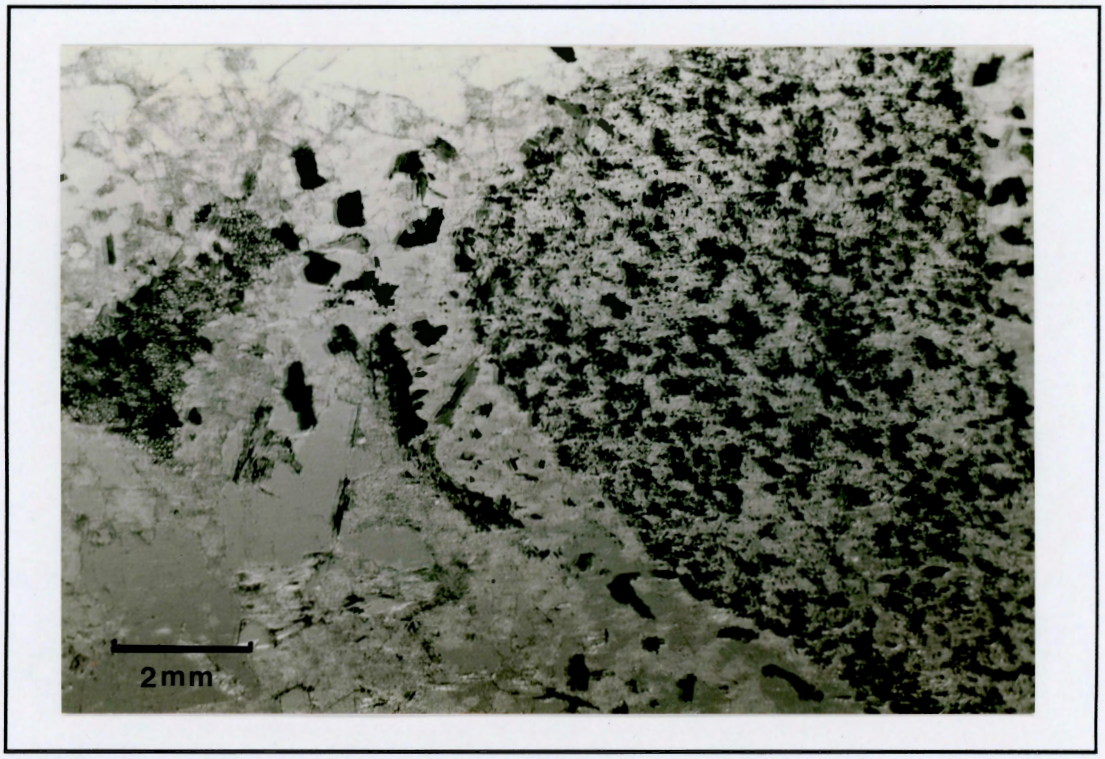

Figure 3.1. TML-8B. Small angular garnet + biotite-rich pelitic enclave and a larger garnet + oxide-rich angular xenolith in a quartz and plagioclase-rich granitic matrix.

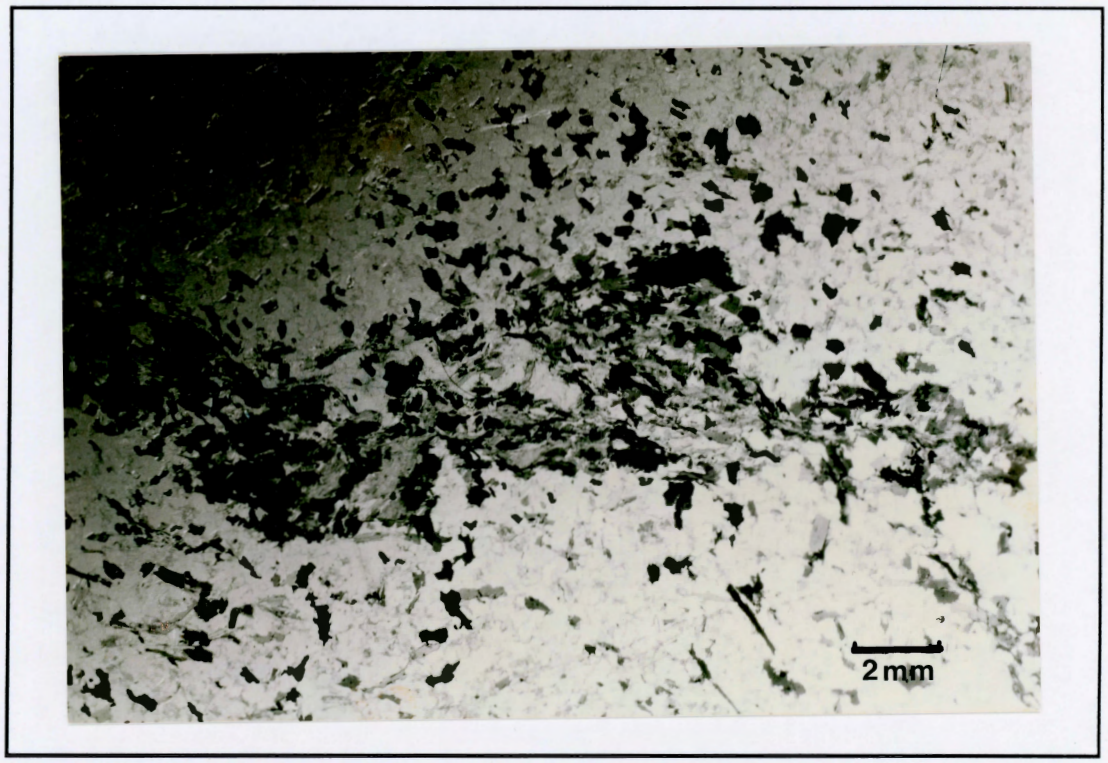

Figure 3.2. TML-7B. Biotite- and fibrolite-rich schlieren in a quartz and plagioclase-rich granitic matix.

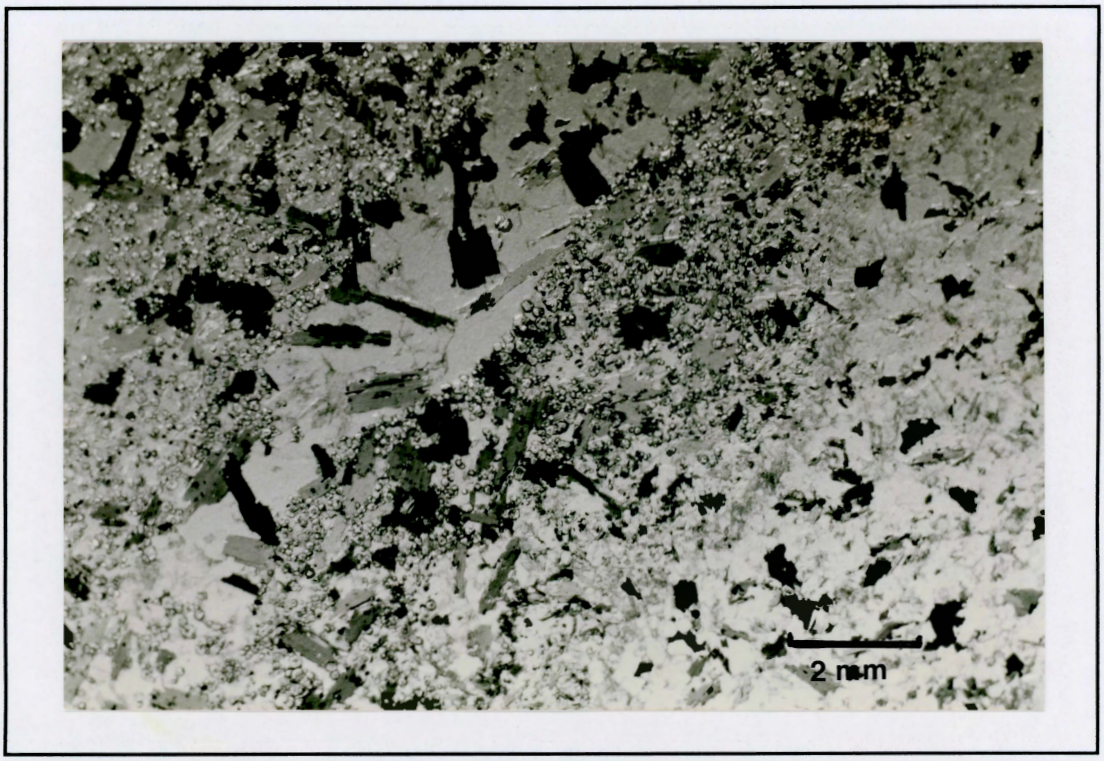

Figure 3.3. TML-3A. Garnet and biotite-rich layers have sharp boundaries with a quartz-rich layer within the enclave and less distinct boundaries against the plagioclase and quartz-rich matrix.

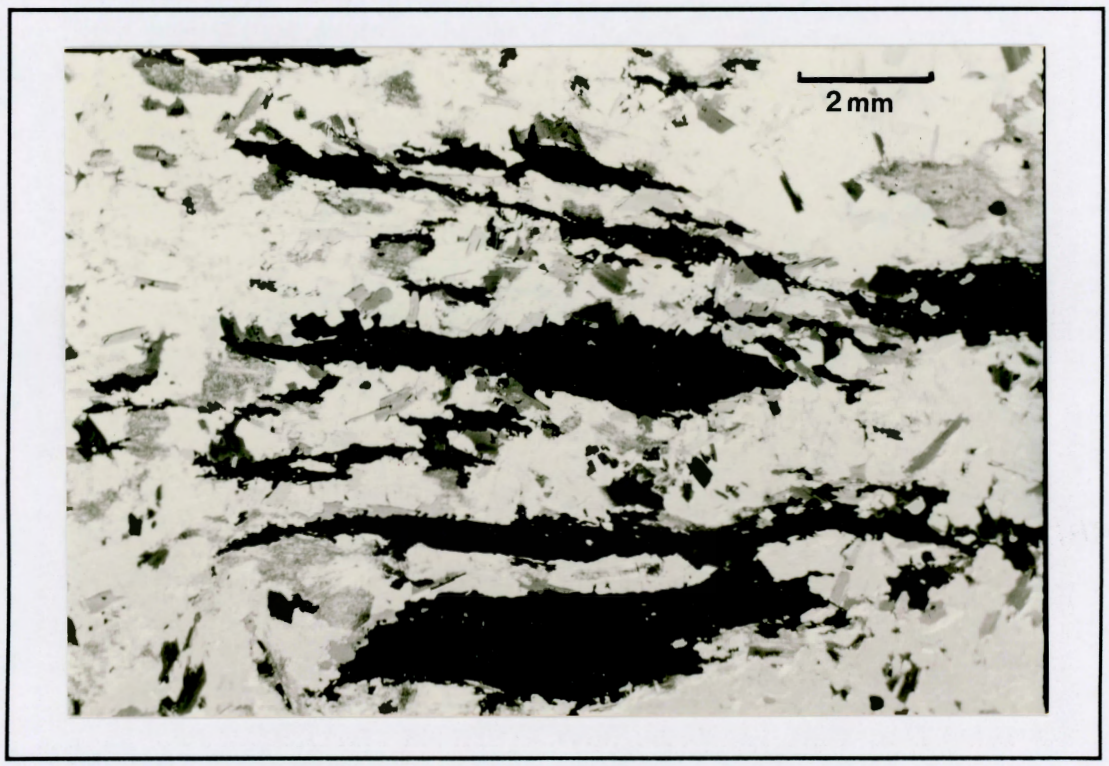

Figure 3.4. TML-6D. Sulfide stringers of pyrite and minor chalcopyrite associated with biotite and within a granitic matrix.

an enclave in a plagioclase and quartz-rich matrix. Pyrite and minor chalcopyrite occur within the matrix as disseminated grains, embayed grains up to 1 cm, and stringers 1 x 10 mm(Fig. 3.4) which are generally rimmed by biotite and/or and garnet and fibrolite. Veinlets filled by carbonate, quartz, and oxides (Fig. 3.5), are evidence for presence of fluids.

Hybrids. Hybrid enclaves typically contain rounded calc-silicate nodules and pelitic enclaves in a granitic host. The TML-8D enclave exhibits a gradational mineral zonation from a carbonate-, clinozoisite- and sphene-rich core to a grossular and amphibole assemblage at a sharp contact with the host (Fig. 3.6). The TML-1B enclave shows no zonation of the calc-silicate and is similar in composition to the calc-silicate enclave, TML-1A, described below. Transfer of fluid is especially clear for the calc-silicates where fibrolite with epidote is found along boundaries between quartz grains and epidote is present along the pelite-calc-silicate boundary in sharp contact with quartz.

Hybrid with quartz. The TML-6A enclave contains calc-silicate minerals within a round, coarse grained quartz nodule in a pelite (Fig. 3.7). Iron-rich epidote occurs in the vicinity of the pelite while clinozoisite and zoisite dominate toward the core. Zoisite is typically rimmed by clinozoisite and subsequently by epidote, the most abundant epidote-group mineral. The TML-5C enclave (Fig. 3.8) contains a rounded coarse grained quartz inclusion, a large pyrite and chalcopyrite cluster, and a large relict feldspar in a fine grained matrix of biotite, plagioclase, oxides, quartz and fibrolite.

Calc-silicate.The TML-1A enclave shows no zoning and contains epidote. Mineralogy of this calc-silicate enclave includes quartz, plagioclase, grossular, hornblende, dolomite, muscovite, sphene, pyrite, chalcopyrite, Fe-Ti oxides, and chlorite.

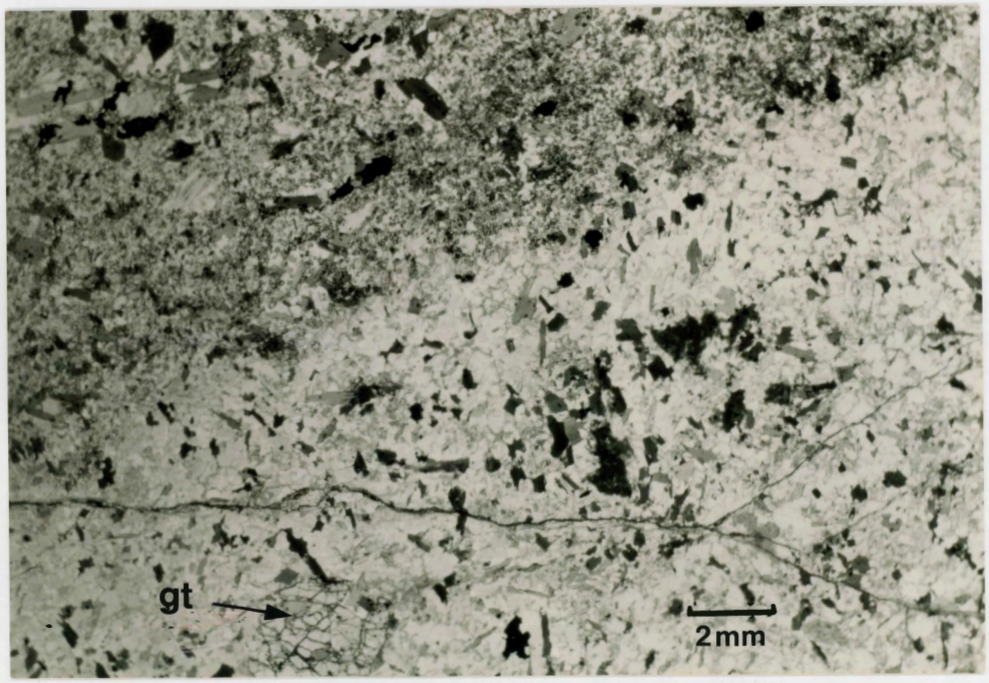

Figure 3.5. TML-8C. Carbonate veinlet, relict garnet with inclusion of biotite and oxides, and angular garnet + biotite-rich xenolith with sericitic alteration.

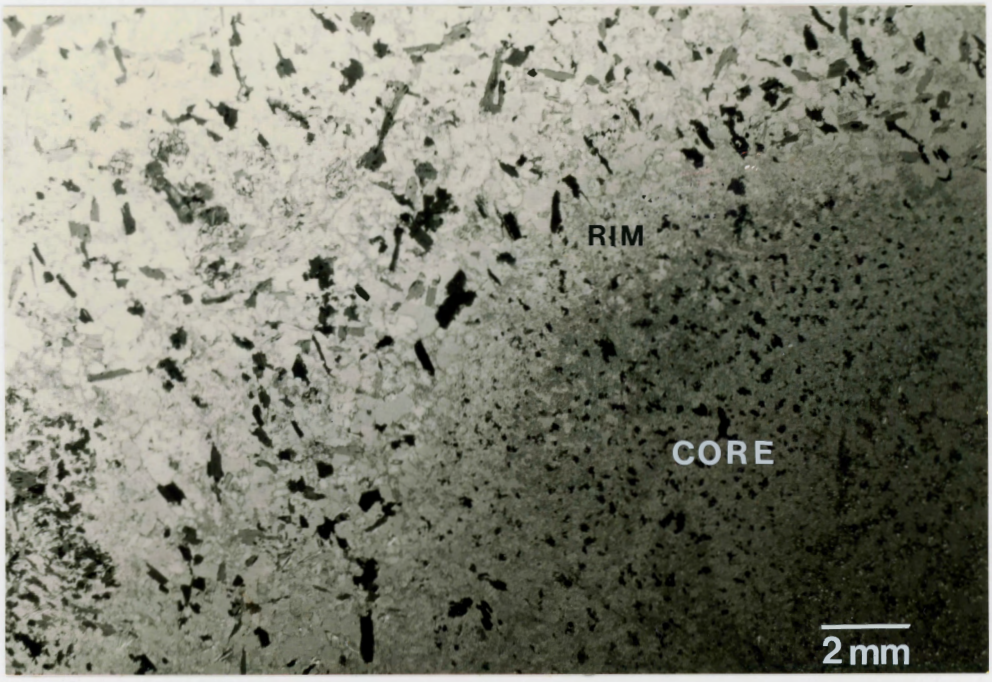

Figure 3.6. TML-8D. Zoned calc-silicate with carbonate + clinozoisite + grossular core grading to an epidote + clinozoisite + zoisite + hornblende rim. The dark area in the lower left corner results from an uneven distibution of the light source during photography.

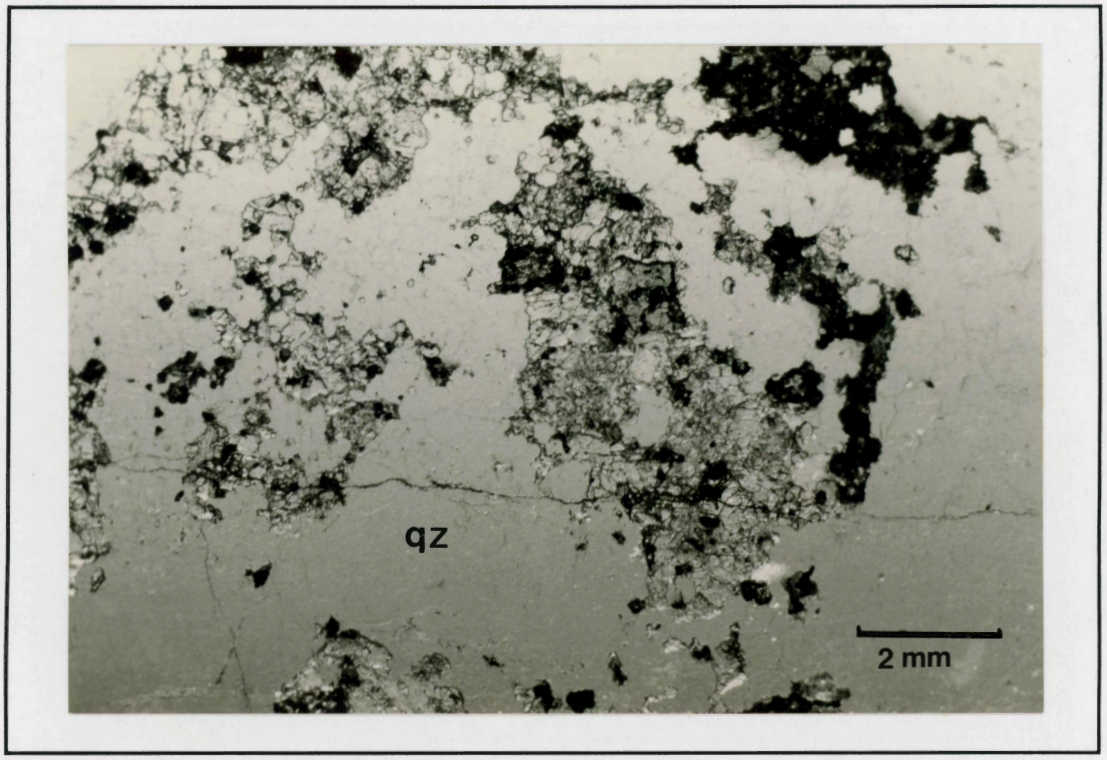

Figure 3. 7. TML-6A.Grossular + clinozoisite + zoisite + epidote + carbonate + amphibole in coarse-grained quartz. Pelite portion of this calc-silicate hybrid is not shown.

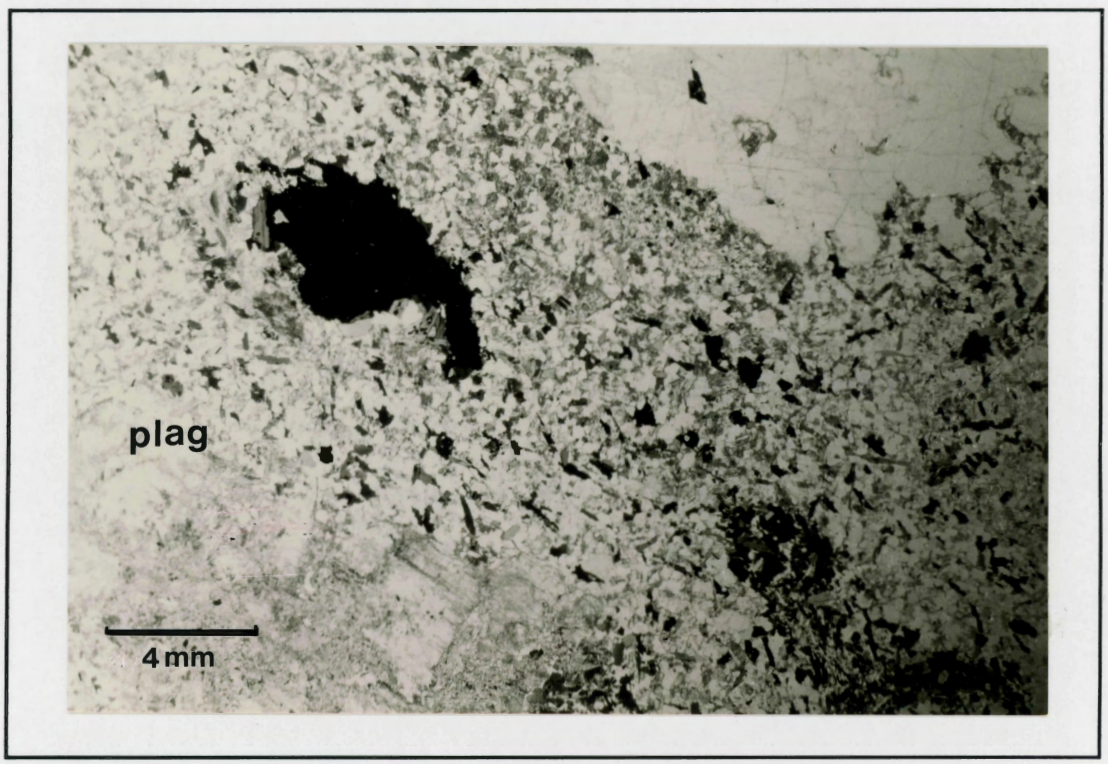

Figure 3. 8. TML-5C. Hybrid with quartz. Quartz nodule (top right), large relict sericitic plagioclase, and pyrite and chalcopyrite (large opaque minerals) rimmed with biotite.

3.3 Mineralogy and Mineral Chemistry

Garnets

Four populations of garnets in the pelitic enclaves are recognized on the basis of textures, inclusions and mineral chemistry. The garnets are classified according to both their Mn content and pre-entrainment or syn-entrainment texture. Mn-poor (0.9-3.0 % Mn) garnets and Mn-rich (6.6-10.4 % Mn) garnets exhibit both pre-entrainment and syn-entrainment textures (i.e. xenoblastic and idioblastic, respectively). The 'A' indicates xenoblastic, xenoblastic and the 'B' indicates idioblastic, idioblastic garnets. The notation '1' and '2' refer to Mn-poor and Mn-rich population, respectively. Figures 3.9 and 3.10 shows Mn-poor pre-entrainment (G1A) and syn-entrainment garnets (G1B), respectively. Figures 3.11 and 3.12 show Mn-rich pre-entrainment (G1A) and syn-entrainment garnets (G1B), respectively. Microprobe traverses of each of the garnets are shown in Figure 3.13.

Garnet G1A

Figure 3.9 shows xenoblastic, relict Mn-poor (0.9-2.5 % Mn) garnet. These garnets are associated with the less mafic enclaves and are unstable with respect to the biotite and plagioclase. A traverse of G1A shows complex zoning from the rim to the core (Fig. 3.13a).

Garnet G1B

Figures 3.5 and 3.10 show subidoblastic garnet up to 1-2 cm with inclusions of Fe-Ti oxides, ± biotite, ± quartz. Microprobe analyses, given in Table 3.1 and illustrated in Figure 13.3b, show that the rims are enriched in Mn with respect to the cores. This is unusual for prograde metamorphism and may represent either retrograde metamorphism or a change in bulk composition of the enclaves resulting from chemical exchange with their host.

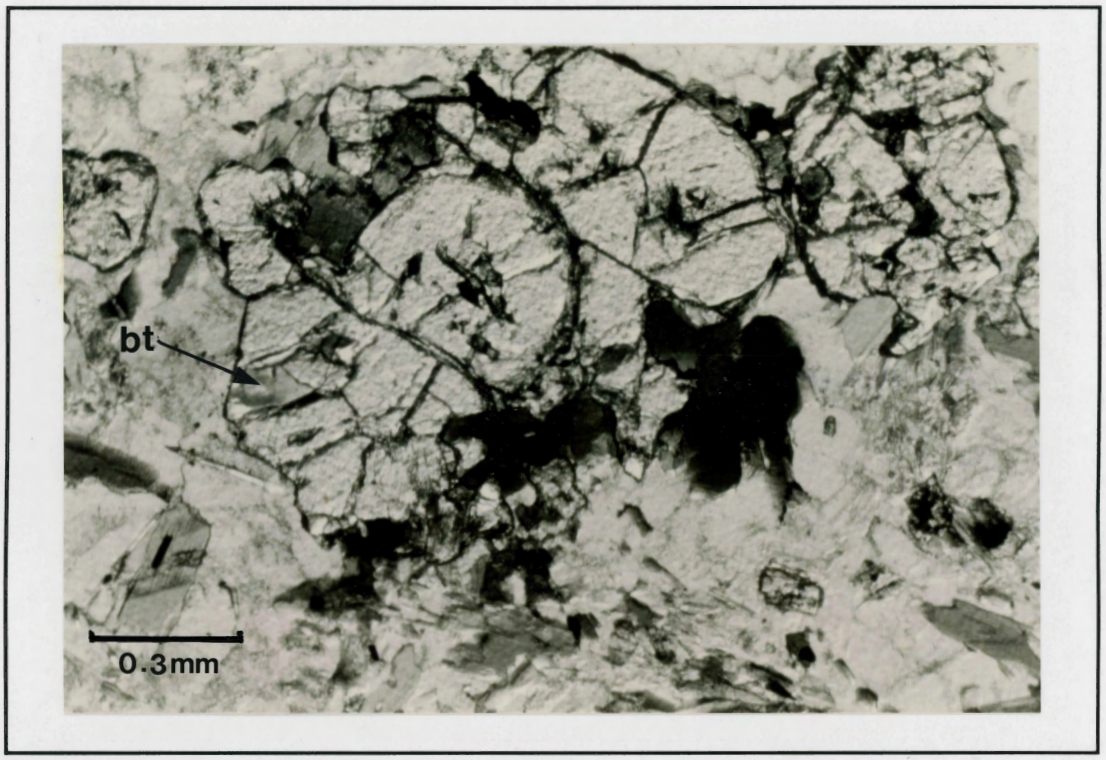

Figure 3.9. G1A in TML-5D: Mn-poor early garnet with inclusions of biotite, quartz, and Fe-Ti oxides.

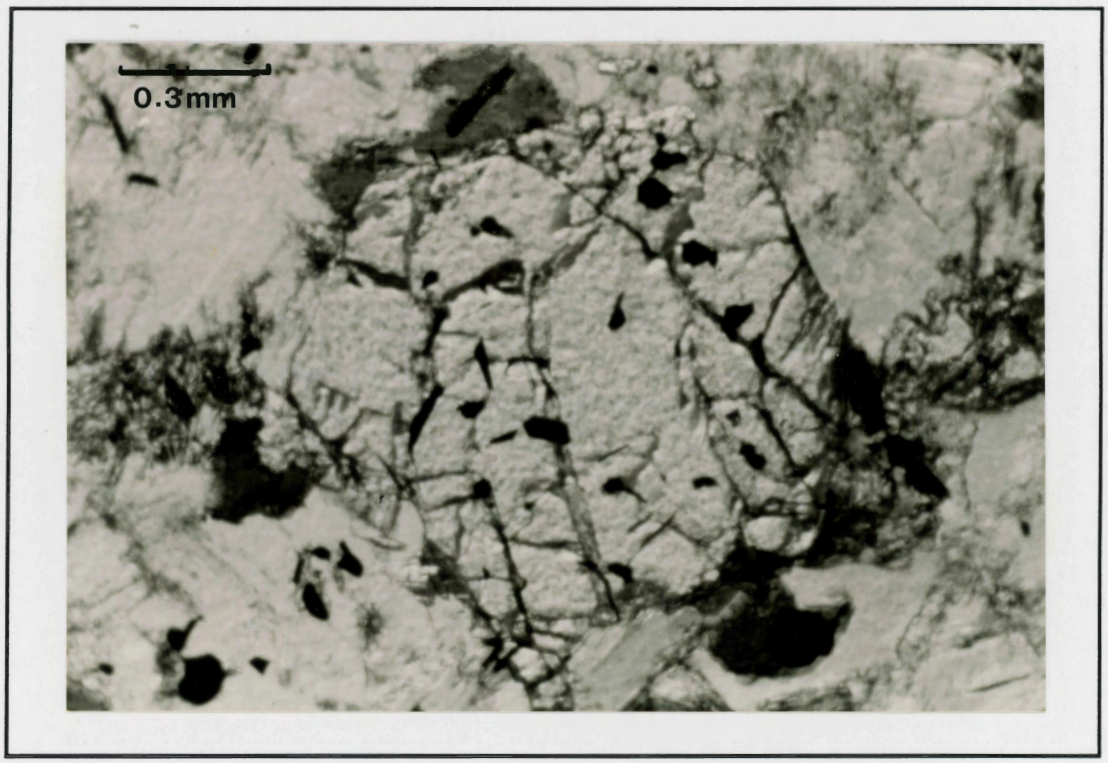

Figure 3. 10. G1B in TML-4B. Mn-poor late garnet with inclusions of Fe-Ti oxides.

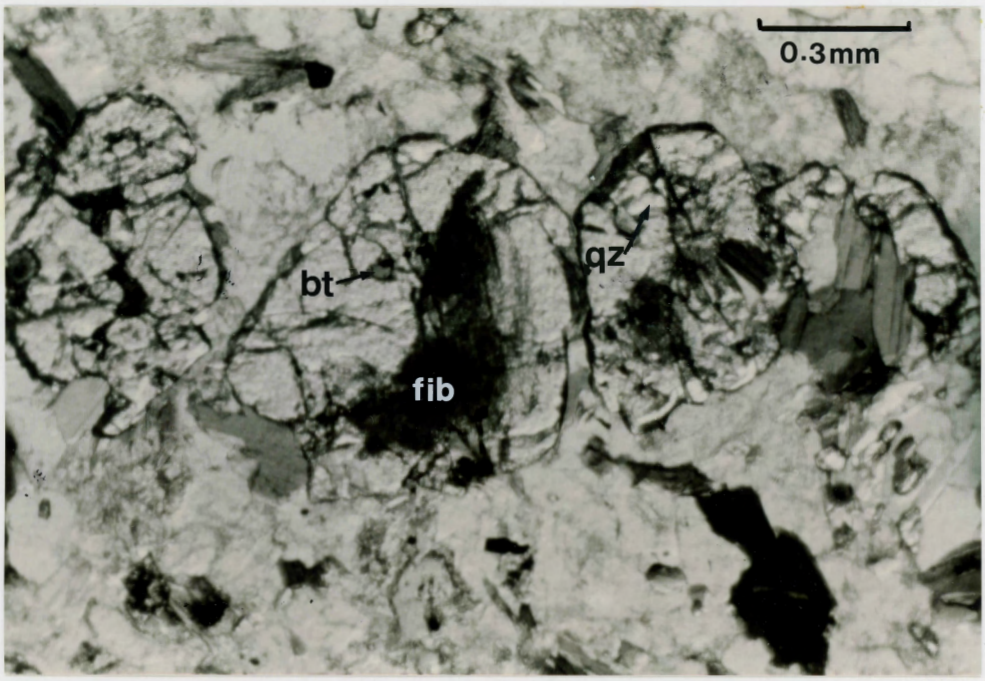

Figure 3. 11. G2A in TML-8C. Mn-rich early garnet with inclusions of biotite, quartz, plagioclase, fibrolite, and Fe-Ti oxides.

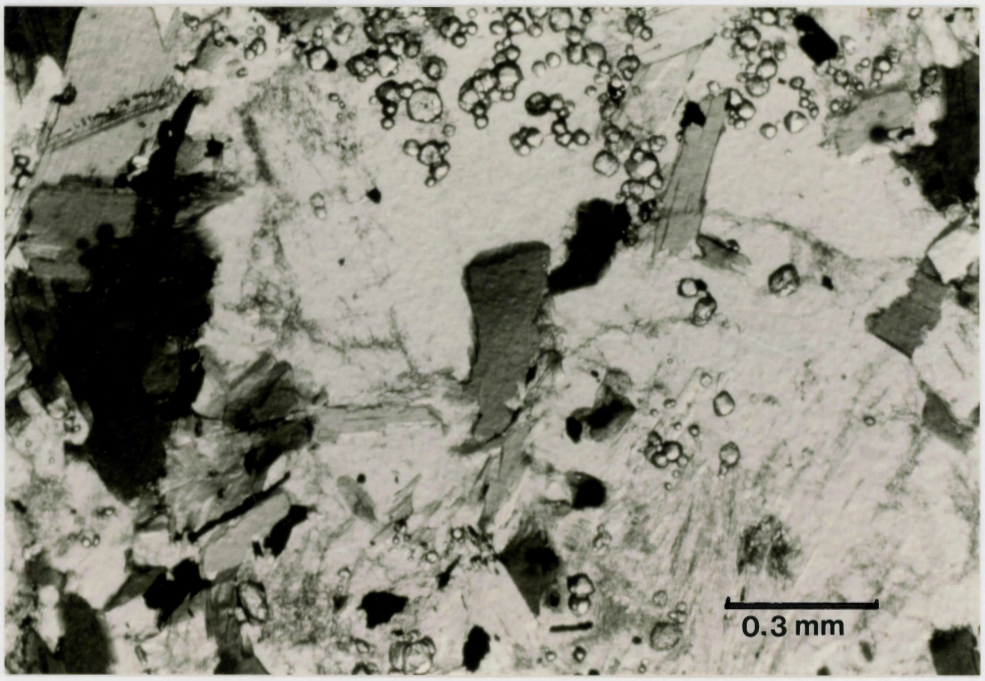

Figure 3.12. G2B in TML-3B. Mn-rich late garnet with quartz inclusions in a matrix of plagioclase, biotite, quartz, and fibrolite.

TABLE 3.1. Microprobe analyses of Mn-poor pre-entrainment (G1A) and syn-entrainment (G1B) garnets with opaque ± biotite and quartz inclusions.

	G1A						G1B				
	1[a]	2[b-1]	3[b-2]	4[b-3]	5[b-4]	6[b-5]	7[a]	8[c-1]	9[c-2]	10[c-3]	11[c-4]
SiO_2	37.74	37.34	37.29	37.05	37.26	36.95	37.53	37.21	37.75	36.62	37.44
TiO_2	0.28	0.05	0.10	0.29	0.17	0.07	0.10	0.24	0.25	0.25	0.12
Al_2O_3	21.01	22.08	22.07	21.85	22.04	21.77	21.84	21.89	21.91	22.11	21.88
Cr_2O_3	0.04	0.03	0.04	0.01	0.02	0.00	0.11	0.03	0.00	0.04	0.00
FeO	31.08	30.64	32.41	33.64	32.96	35.20	31.11	30.37	28.71	30.33	31.87
MnO	2.06	2.50	0.85	2.40	0.90	1.23	2.37	2.96	0.92	1.13	1.17
MgO	6.99	6.26	6.21	4.43	0.62	4.08	6.18	5.71	8.09	7.04	6.52
CaO	1.15	1.17	1.04	1.06	1.06	1.03	1.19	1.73	1.62	1.36	1.24
Na_2O	0.00	0.00	0.00	0.00	0.01	0.00	0.03	0.00	0.00	0.00	0.00
Total	100.35	100.07	100.01	100.73	100.01	100.33	100.46	100.14	99.25	98.88	100.26
				Cations per formula based on 24 oxygens							
Si	5.940	5.889	5.888	5.885	5.898	5.905	5.906	5.883	5.914	5.819	5.893
Al^{IV}	0.060	0.111	0.112	0.115	1.102	0.095	0.094	0.117	0.086	0.181	0.107
Al^{VI}	3.834	3.991	3.992	3.972	4.006	4.003	3.954	3.959	3.956	3.957	3.950
Ti	0.033	0.006	0.012	0.035	0.020	0.008	1.012	0.029	0.030	0.030	0.014
Cr	0.005	0.004	0.005	0.001	0.003	0.00	0.014	0.004	0.000	0.005	0.002
Fe	4.091	4.042	4.280	4.469	4.363	4.705	4.095	4.016	3.761	4.031	4.196
Mn	0.275	0.334	0.114	0.323	0.121	0.167	0.316	0.396	0.122	0.152	0.156
Mg	1.640	1.471	1.461	1.049	1.326	0.972	1.449	1.345	1.889	1.667	1.465
Ca	0.194	0.198	0.176	0.180	0.180	0.176	0.201	0.293	0.272	0.232	0.209
Na	0.000	0.000	0.000	0.000	0.003	0.000	0.009	0.000	0.000	0.000	0.000
Alm	0.660	0.669	0.710	0.742	0.728	0.782	0.676	0.664	0.662	0.663	0.720
Gr	0.031	0.033	0.029	0.030	0.030	0.029	0.033	0.048	0.045	0.038	0.034
Py	0.265	0.243	0.242	0.174	0.221	0.161	0.239	0.222	0.313	0.274	0.251
Sp	0.044	0.055	0.019	0.054	0.020	0.028	0.052	0.065	0.020	0.025	0.026

a: TML - 3B b: TML - 8C (b-1: rim to b-5: core) c:TML - 4B (c-1: rim to c-4: core)

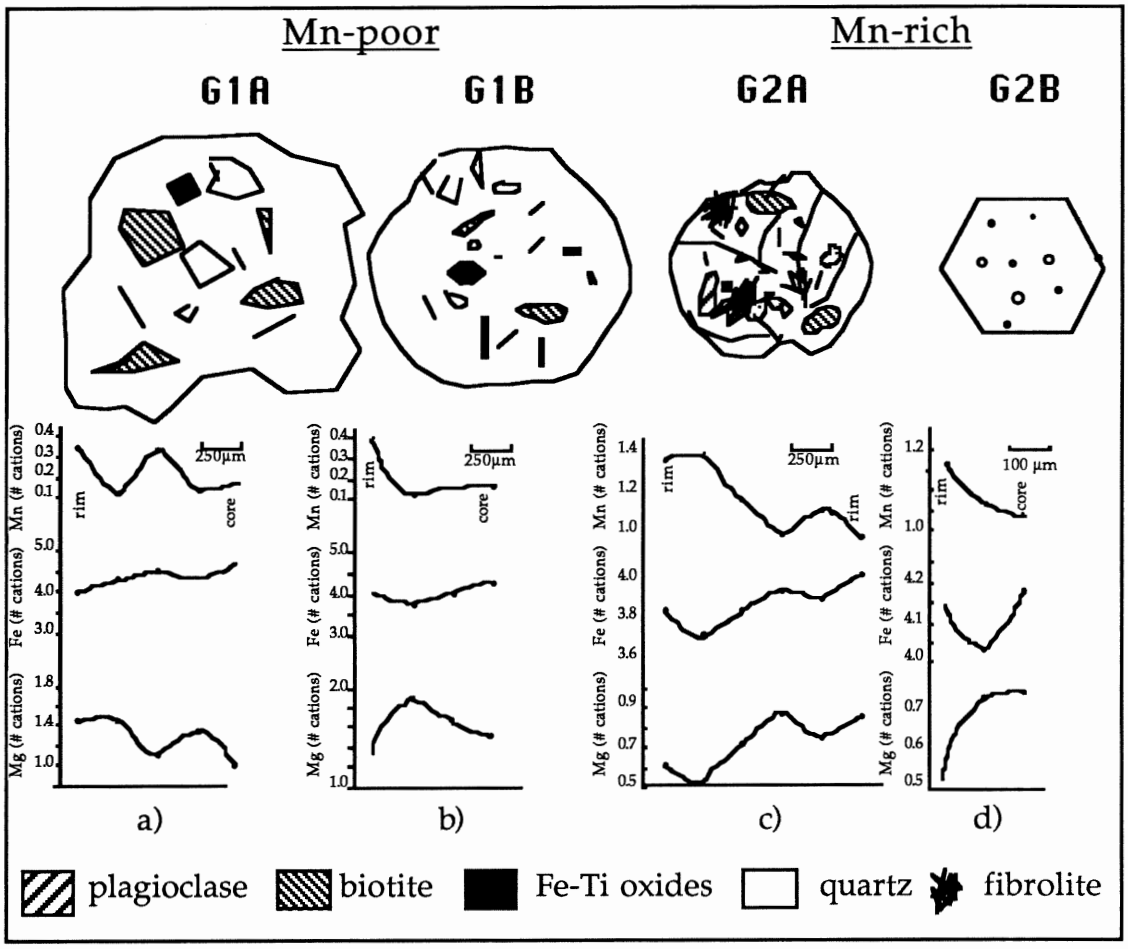

Figure 3.13 Garnet traverses a) G1A: Mn-poor, xenoblastic, with complex chemical zonation. Rim to core are based on analyses 2 to 6 from Table 3.1 with complex zonation. b) G1B: Mn-poor, idioblastic with strong reversed zonation at the rim. Rim to core are based on analyses 8 to 11 from Table 3.1. c) G2A: Mn-rich, xenoblastic with complex chemical zonation. Rim to rim are based on analyses 6 to 11 from Table 3.2. d) G2B: rim to core are based on analyses 5 to 7 from Table 3.3. Garnets. Note the change in scale for (c) garnets.

Garnet G2A

Mn-rich garnets in the most mafic enclaves contain inclusions of biotite, plagioclase, quartz, fibrolite, and Fe-Ti oxides (Fig. 3.10; Table 3.2). These garnets are sub-idioblastic, but are often fractured and resorbed similar to G1A. The pyrope and almandine component of garnet generally increase, whereas the spessartine component generally decreases with increasing metamorphic grade.

TABLE 3.2. Microprobe analyses of pre-entrainment Mn-rich garnets with biotite, plagioclase, fibrolite and quartz ± Fe-Ti oxide inclusions

	1[a]	2[a]	3[b]	4[c]	5[d]	6[b-1]	7[b-2]	8[b-3]	9[b-4]	10[b-5]	11[b-6]
SiO_2	37.15	36.98	36.61	36.67	36.67	36.65	37.34	36.36	36.41	36.9	37.05
TiO_2	0.08	0.15	0.10	0.05	0.05	0.00	0.06	0.02	0.07	0.10	0.04
Al_2O_3	20.56	20.80	21.71	21.66	20.85	21.84	21.59	21.43	21.14	21.36	21.69
Cr_2O_3	0.07	0.09	0.03	0.04	0.05	0.00	0.00	0.01	0.02	0.05	0.02
FeO	29.93	30.59	27.60	29.59	28.21	28.55	27.79	28.10	28.87	28.88	30.00
MnO	8.03	7.27	10.38	7.85	8.58	9.65	10.19	8.30	7.04	7.97	7.05
MgO	3.22	3.35	2.18	3.21	2.77	2.52	2.22	2.96	3.62	3.04	3.53
CaO	1.22	1.13	1.80	1.22	1.89	1.35	1.90	1.25	1.12	1.13	1.13
Na_2O	0.00	0.00	0.00	0.00	0.09	0.00	0.00	0.05	0.00	0.00	0.00
Total	100.29	100.36	100.41	100.29	99.23	100.56	101.09	98.48	98.28	99.43	100.51
					Cations per formula based on 24 oxygens						
Si	5.991	5.956	5.903	5.897	5.965	5.896	5.968	5.937	5.943	5.966	5.925
Al^{IV}	0.009	0.044	0.097	0.103	0.035	0.104	0.032	0.063	0.057	0.034	0.075
Al^{VI}	3.895	3.901	4.025	3.999	3.961	4.035	4.032	4.058	4.007	4.034	4.010
Ti	0.010	0.018	0.012	0.006	0.006	0.000	0.007	0.002	0.009	0.012	0.005
Cr	0.009	0.011	0.004	0.005	0.006	0.000	0.000	0.001	0.003	0.006	0.003
Fe	4.036	4.120	3.722	3.979	3.840	3.841	3.714	3.837	3.941	3.905	4.012
Mn	1.097	0.992	1.418	1.069	1.183	1.315	1.379	1.148	0.973	1.092	0.955
Mg	0.774	0.804	0.524	0.769	0.672	0.604	0.529	0.720	0.881	0.733	0.841
Ca	0.211	0.195	0.311	0.210	0.330	0.233	0.325	0.219	0.196	0.196	0.194
Na	0.009	0.000	0.000	0.000	0.000	0.000	0.000	0.000	0.000	0.000	0.000
Alm	0.662	0.674	0.623	0.660	0.637	0.641	0.625	0.648	0.678	0.659	0.668
Gr	0.035	0.032	0.052	0.035	0.055	0.039	0.055	0.037	0.033	0.033	0.032
Py	0.127	0.132	0.088	0.128	0.112	0.101	0.089	0.122	0.147	0.124	0.140
Sp	0.180	0.162	0.237	0.177	0.196	0.219	0.232	0.194	0.162	0.184	0.159

a: TML - 3B b:TML - 4B (b-1: rim to b-6: rim) c: TML - 8B d: TML - 8D

The spessartine component increases from the core to the rim before finally decreasing. The unusual rise in almandine and pyrope at the rims may represent a change in pressure and temperature conditions during the growth of the garnet or may suggest a change in bulk chemistry. The asymmetry may suggest that the traverse does not represent a section through the true core and that the original rim at both sides may not have remained intact.

Garnet G2B

Idioblastic, Mn-rich garnets reach up to 300 μm in diameter, and contain small inclusions of quartz (Table 3.3; Figure 3.12). They tend to occur in clusters where G2B dominates (Fig. 3.3) and are associated with biotite, plagioclase, quartz and fibrolite in the matrix. These garnets show an enrichment of spessartine component from the core to rim similar to that observed for the G1B garnets. In general, Mn and Ca increase toward the rim while Mg decreases rapidly and iron first decreases before finally increasing.

Grossular

Table 3.4 shows two microprobe analyses of grossular in the calc-silicate of TML-8D. The grossular component ranges from 80 % and 88 %. The andradite component, calculated from the total FeO, represents about half of the total Fe in the garnet.

Plagioclase

Minor chessboard twinning, attributed to the albitization of feldspars, is evident in plagioclase up to 3 mm (Fig. 3.14). Idioblastic to sub-idioblastic zoned plagioclase (up to 4 mm), commonly has sericitized cores, and rims of twinned and untwinned plagioclase (Fig. 3.15).

Xenoblastic, simple albite-twinned and untwinned plagioclase grains are included in G2A, and occur throughout the matrix both as rims on earlier

TABLE 3.3. Microprobe analyses of Mn-rich syn-entrainment small garnets with quartz inclusions.

	1[a]	2[a]	3[a]	4[a-1]	5[a-2]	6[a-3]	7[b]	8[b]	9[c]	10[c]	11[c]
SiO_2	37.06	36.95	36.70	36.73	36.11	36.79	36.66	36.89	36.71	37.13	37.19
TiO_2	0.07	0.11	0.07	0.06	0.21	0.24	0.06	0.13	0.11	0.10	0.07
Al_2O_3	21.30	21.67	20.49	20.69	21.44	20.97	21.68	21.56	21.45	21.15	20.72
Cr_2O_3	0.07	0.01	0.07	0.12	0.15	0.10	0.02	0.14	0.11	0.08	0.04
FeO	30.32	30.44	30.78	30.49	29.67	30.43	28.35	28.20	31.05	30.59	30.21
MnO	8.47	8.10	8.22	8.52	7.51	7.47	8.95	8.11	6.81	6.61	6.64
MgO	2.27	2.68	2.38	2.13	3.03	3.09	2.95	3.14	2.90	3.21	3.09
CaO	1.34	1.23	1.15	1.31	0.92	0.71	1.02	1.43	1.51	1.58	2.16
Total	100.29	101.19	99.86	100.05	99.04	99.80	99.70	99.60	100.65	100.45	100.42
					Cations per formula based on 24 oxygens						
Si	5.991	5.911	5.979	5.973	5.882	5.953	5.922	5.945	5.900	5.958	5.978
Al^{IV}	0.009	0.089	0.021	0.027	0.118	0.047	0.078	0.055	0.100	0.042	0.022
Al^{VI}	3.895	3.993	3.911	3.936	3.995	3.950	4.047	4.036	3.960	3.955	3.901
Ti	0.009	0.013	0.009	0.007	0.026	0.030	0.007	0.016	0.013	0.012	0.009
Cr	0.009	0.001	0.009	0.015	0.019	0.013	0.003	0.018	0.014	0.010	0.005
Fe	4.075	4.072	4.194	4.147	4.042	4.118	3.830	3.800	4.174	4.105	4.061
Mn	1.153	1.098	1.134	1.174	1.036	1.024	1.225	1.107	0.927	0.898	0.904
Mg	0.544	0.639	0.578	0.516	0.736	0.745	0.710	0.745	0.695	0.768	0.740
Ca	0.231	0.211	0.201	0.228	0.161	0.123	0.177	0.247	0.260	0.272	0.424
Alm	0.679	0.676	0.687	0.684	0.676	0.685	0.645	0.643	0.689	0.679	0.663
Gross	0.038	0.035	0.033	0.038	0.017	0.020	0.030	0.042	0.043	0.045	0.069
Pyr	0.091	0.106	0.095	0.085	0.123	0.124	0.119	0.128	0.115	0.127	0.120
Spess	0.192	0.182	0.186	0.194	0.173	0.170	0.206	0.187	0.153	0.149	0.147

a: TML - 3B (a-1: rim to a-3: core) b: TML - 8B c: TML - 8C

TABLE 3.4. Microprobe analyses of grossular in TML - 8D calc-silicate nodule

	1	2
SiO_2	38.45	38.75
TiO_2	0.08	0.34
Al_2O_3	20.85	21.02
Cr_2O_3	0.00	0.00
FeO	6.06	4.13
MnO	2.29	0.82
MgO	0.12	0.11
CaO	31.78	35.20
Na_2O	0.00	0.00
K_2O	0.00	0.00
Total	99.63	100.37
Cations per formula based on 24 oxygens		
Si	5.948	5.915
Al^{IV}	0.052	0.085
Al^{VI}	3.747	3.695
Ti	0.009	0.039
Cr	0.000	0.000
Fe	0.784	0.527
Mn	0.300	0.106
Mg	0.028	0.025
Ca	5.268	5.758
Na	0.000	0.000
Alm	0.047	0.086
And	0.057	0.063
Gr	0.875	0.798
Py	0.004	0.005
Sp	0.017	0.049

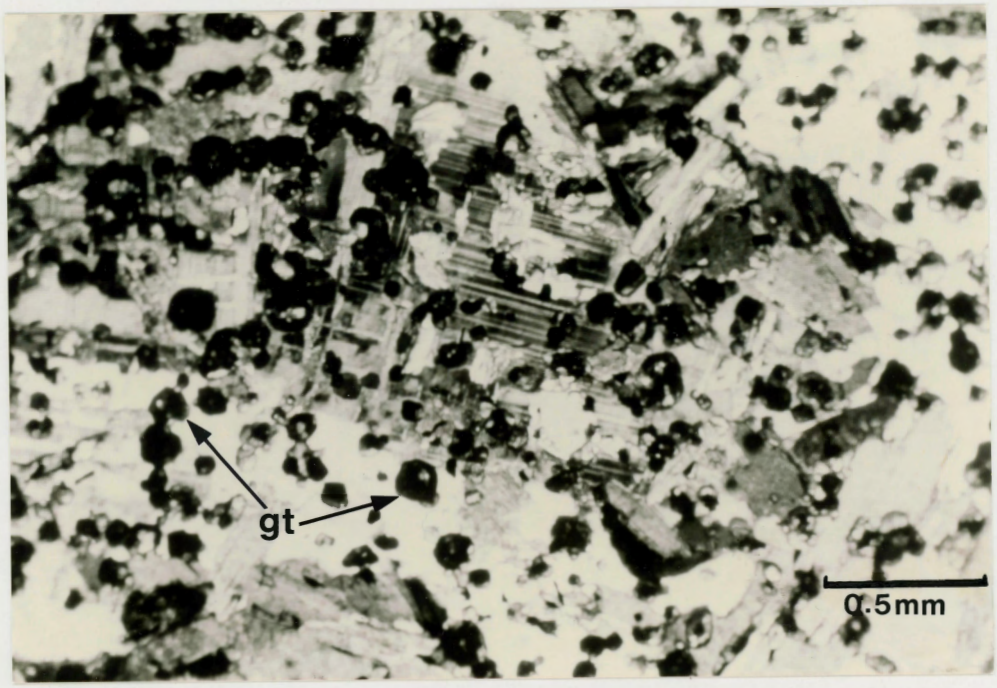

Figure 3. 14. TML-3A. Chessboard twinning in plagioclase with abundant G2B.

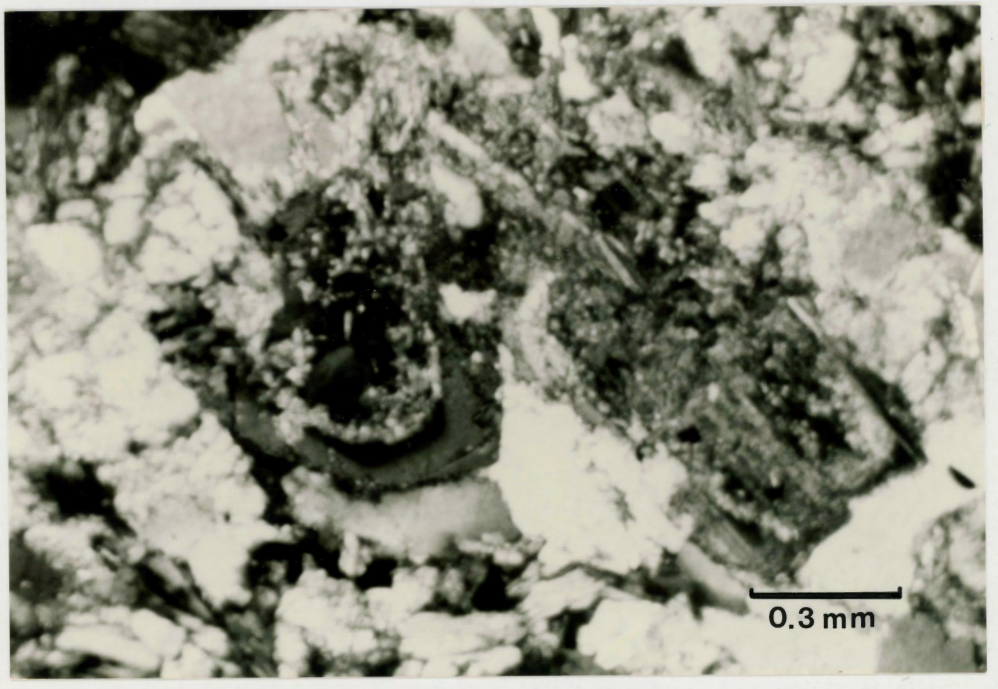

Figure 3.15. TML-3A. Relict feldspars showing complex zoning and intermediate rim-core sericitization.

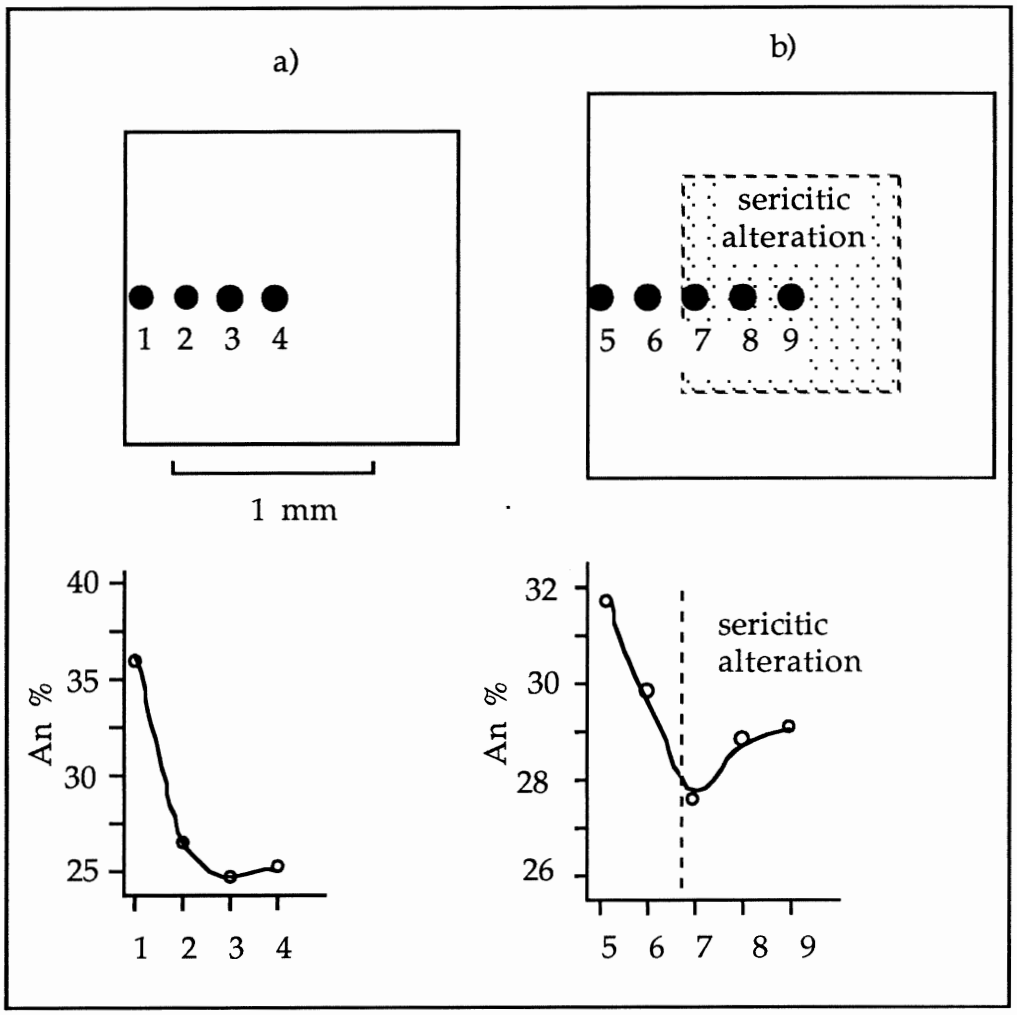

Figure 3.16. Plagioclase traverses. a) an unaltered plagioclase plotted from analyses 1-4, Table 3.5 b) plagioclase with sericitic core plotted from analyses 5-9, Table 3.5. Both show normal zoning in the core and reverse zoning in the rim.

plagioclase and as interstitial material.

Microprobe data for large plagioclase rimmed with late plagioclase are tabulated in Table 3.5 and the corresponding anorthite content is plotted in Figure 3.16. Both plagioclases show normal zoning in the core and a strong reverse zoning in the rim.

Table 3.6 lists microprobe analyses for small anhedral matrix plagioclases and one plagioclase inclusion in G2A garnet. The cores have anorthite content of 31-

TABLE 3.5. Microprobe analyses of plagioclase; normally zoned cores with reverse rims

	1	2	3	4	5	6	7	8	9
SiO_2	57.77	61.14	61.34	61.16	59.98	60.69	61.06	60.99	60.30
Al_2O_3	25.52	25.22	24.82	24.91	25.43	25.50	24.10	24.59	25.03
FeO	0.10	0.05	0.01	0.01	0.12	0.12	0.23	0.27	0.30
CaO	7.74	5.67	5.40	5.45	6.56	6.21	5.6	5.88	5.96
Na_2O	7.47	8.86	8.95	8.71	7.86	8.13	8.66	8.22	8.29
K_2O	0.10	0.00	0.00	0.00	0.00	0.00	0.00	0.00	0.00
Total	98.60	100.94	100.52	100.24	99.95	100.65	99.75	99.95	99.88
	Cations per formula based on 32 oxygens								
Si	10.483	10.774	10.842	10.833	10.682	10.723	10.887	10.845	10.748
Al	5.454	5.234	5.167	5.196	5.334	5.306	5.061	5.150	5.254
Fe	0.015	0.007	0.001	0.001	0.018	0.018	0.034	0.040	0.045
Ca	1.505	1.071	1.023	0.034	1.252	1.176	1.070	1.120	1.138
Na	2.628	3.027	3.067	2.991	1.714	2.785	2.994	2.834	2.865
K	0.023	0.000	0.000	0.000	0.000	0.000	0.000	0.000	0.000
Ab	63.00	73.74	74.97	74.28	68.13	70.00	72.59	70.95	70.78
An	36.44	26.26	25.03	25.72	31.87	30.00	27.41	29.05	29.22

Analyses 1 (rim) to 4 (core) of plagioclase TML-3B

Analyses 5 (rim) to 9 (core) of plagioclase TML-3B

TABLE 3.6. Microprobe analyses of anhedral normally zoned plagioclase with three rim to core comparisons.

	1[a-1]	2[b-1]	3[c-2]	4[d-2]	5[e-3]	6[f-3]	7[a]	8[c]	9[c]	10[c]	11[g]
SiO_2	62.56	58.34	61.58	59.83	62.33	58.47	61.61	60.82	61.71	61.58	59.03
Al_2O_3	23.44	26.20	24.23	26.03	23.62	25.07	24.32	25.55	25.40	24.23	25.98
FeO	0.07	0.04	0.09	0.02	0.02	0.03	0.20	0.02	0.02	0.09	0.15
MnO	0.00	0.00	0.00	0.00	0.00	0.00	0.00	0.00	0.00	0.00	0.00
MgO	0.00	0.00	0.00	0.00	0.00	0.00	0.00	0.00	0.00	0.00	0.00
CaO	5.77	8.35	5.00	6.64	4.88	8.06	6.10	5.98	5.68	5.00	7.37
Na_2O	7.11	6.56	8.93	8.05	7.45	6.80	8.17	7.60	7.39	8.93	7.64
Total	98.95	99.49	99.83	100.57	98.30	98.43	100.40	99.97	100.20	99.83	100.17
					Cations per formula based on 32 oxygens						
Si	11.140	10.467	10.942	10.600	11.149	10.599	10.901	10.776	10.874	10.942	10.527
Al	4.916	5.536	5.070	5.431	4.976	5.352	5.068	5.331	5.271	5.070	5.457
Fe	0.010	0.006	0.013	0.003	0.003	0.005	0.030	0.003	0.003	0.013	0.022
Mn	0.000	0.000	0.000	0.000	0.000	0.000	0.000	0.000	0.000	0.000	0.000
Mg	0.000	0.000	0.000	0.000	0.000	0.000	0.000	0.000	0.000	0.000	0.000
Ca	1.101	1.605	0.952	1.260	0.935	1.566	1.156	1.135	1.072	0.952	1.408
Na	2.455	2.282	3.077	2.765	2.390	2.765	2.803	2.611	2.525	3.077	2.642
Ab	68.84	58.62	76.12	68.64	73.36	60.35	70.19	69.64	70.13	76.12	64.87
An	31.16	41.38	23.88	31.36	26.64	39.65	29.70	30.36	29.87	23.88	35.13

a: rim composition of TML-3B
b: core composition of TML-3B
c: rim composition of TML-4B
d: core composition of TML-4B
e: rim composition of TML-6B
f: core composition of TML-6B
g: rim of inclusion in G2A, TML-3B

41 % and rims of 24-31 %. Analysis 118 is from an inclusion in a G2A garnet and has an anorthite composition of 35 %, higher than that of the rims of matrix plagioclase but comparable the to An content of the cores of anhedral matrix plagioclase and to the rim content of large complexly zoned plagioclase. The large plagioclases have normal zoning in the core which reverses in the rim.

Aluminum silicate minerals

Relict phases

Relict kyanite only occurs with sillimanite. Relict kyanite and sillimanite are shown in Figures 3.17 and 3.18. Both react to form sericite-rich rims, and are commonly associated with new fibrolite. Fibrolite commonly replaces biotite (Fig. 3.19). Sillimanite and kyanite occur as xenocrysts in the matrix. Relict kyanite and sillimanite in the matrix indicates that higher pressures and/or lower temperature conditions were responsible for the formation of coarse aluminum silicates and xenoblastic to sub-idioblastic garnets during an early metamorphism.

Stable phase

Fibrolite is ubiquitous in the pelitic enclaves. It occurs as inclusions in garnet (Fig. 3.11) as well as in the matrix where it directly replaces biotite, muscovite (Fig.s 3.20 and 3.21), and plagioclase. Fibrolite is associated with rapid growth and is believed to represent a disordered protosillimanite (Kerrick, 1987). The presence of fibrolite in the matrix and as inclusions in relict garnets, suggests that sillimanite was the stable aluminum silicate during both pre-entrainment and syn-entrainment metamorphism.

Biotite

Biotite is a major component in all of the pelitic enclaves as inclusions in garnet and throughout the matrix. It occurs as a relict phase pseudomorphed by

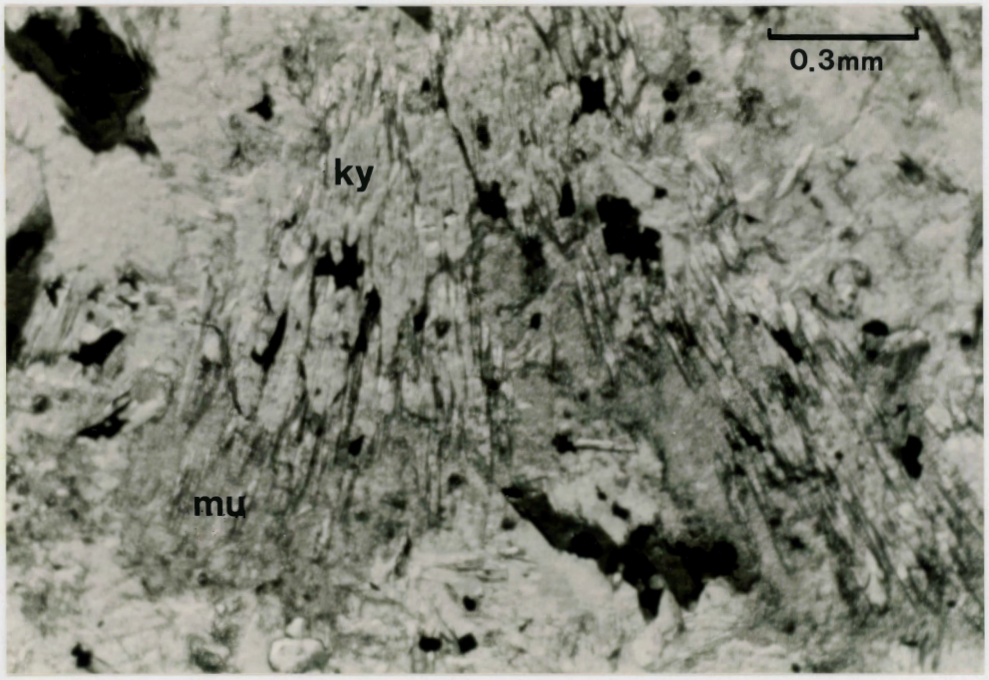

Figure 3.17. TML-3B. Relict kyanite rimmed with fine grained muscovite.

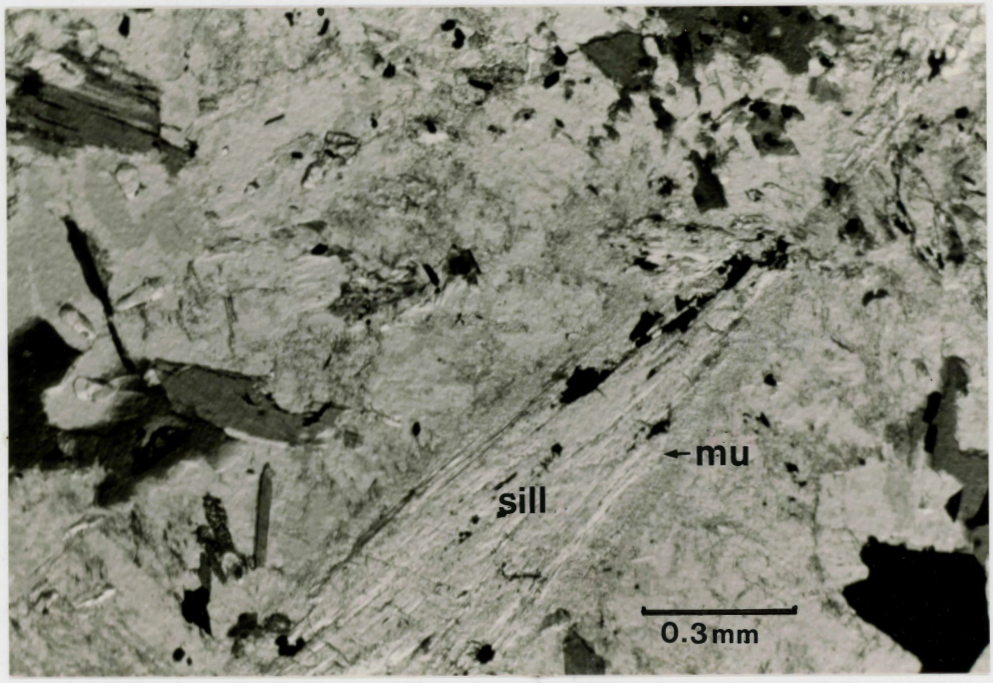

Figure 3.18. TML-3B. Relict coarse sillimanite rimmed with fine grained muscovite

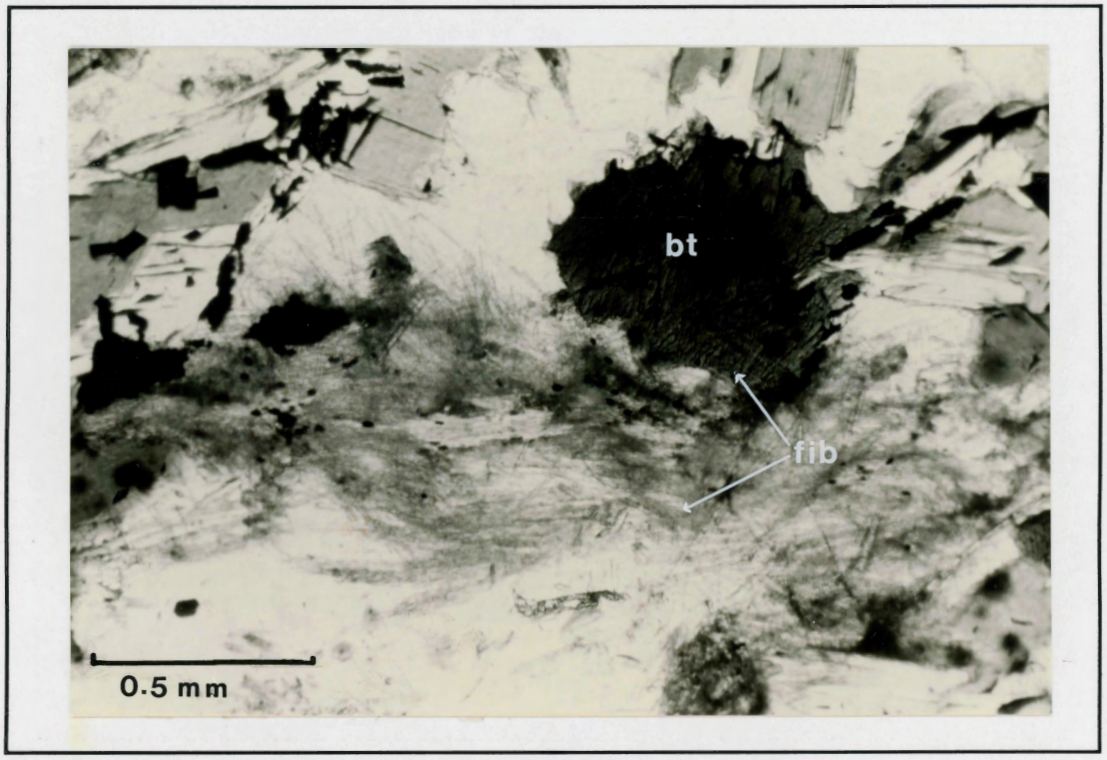

Figure 3.19. TML-6B. Late fibrolite with oxides replacing biotite.

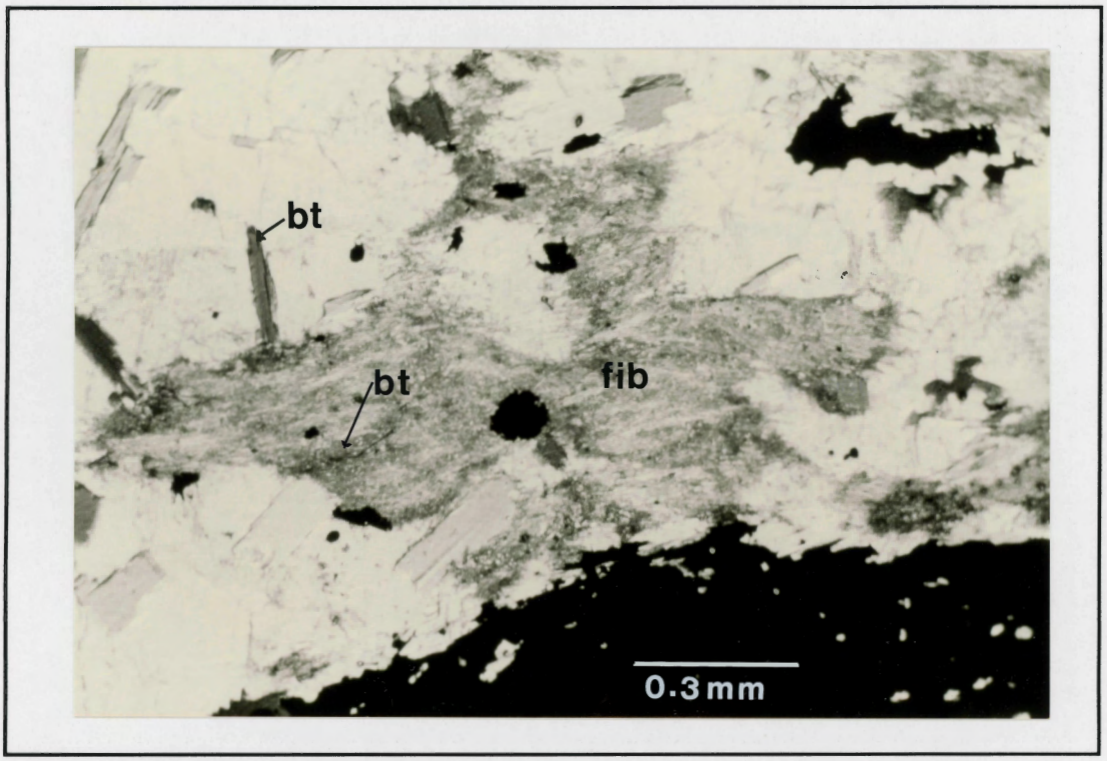

Figure 3.20. TML-6D. Fibrolite has extensively replaced early biotite while late idioblastic biotite is unaffected.

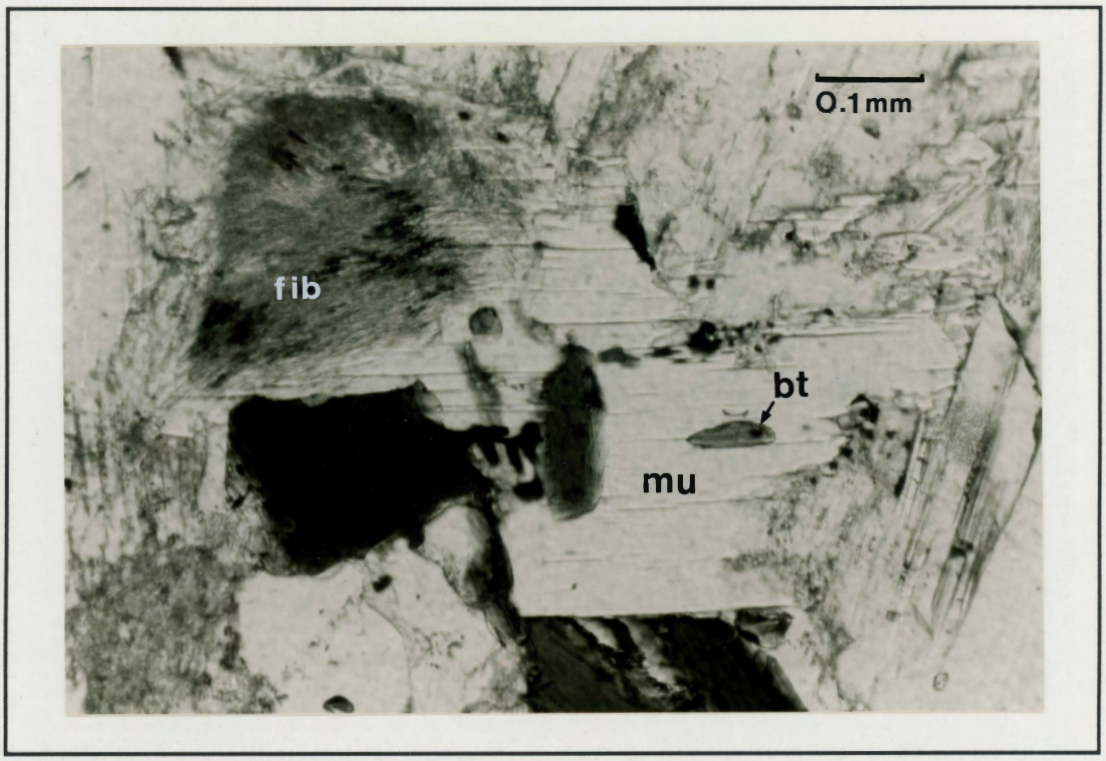

Figure 3.21. TML-6D. Secondary muscovite containing inclusions of early biotite and nucleation of fibrolite

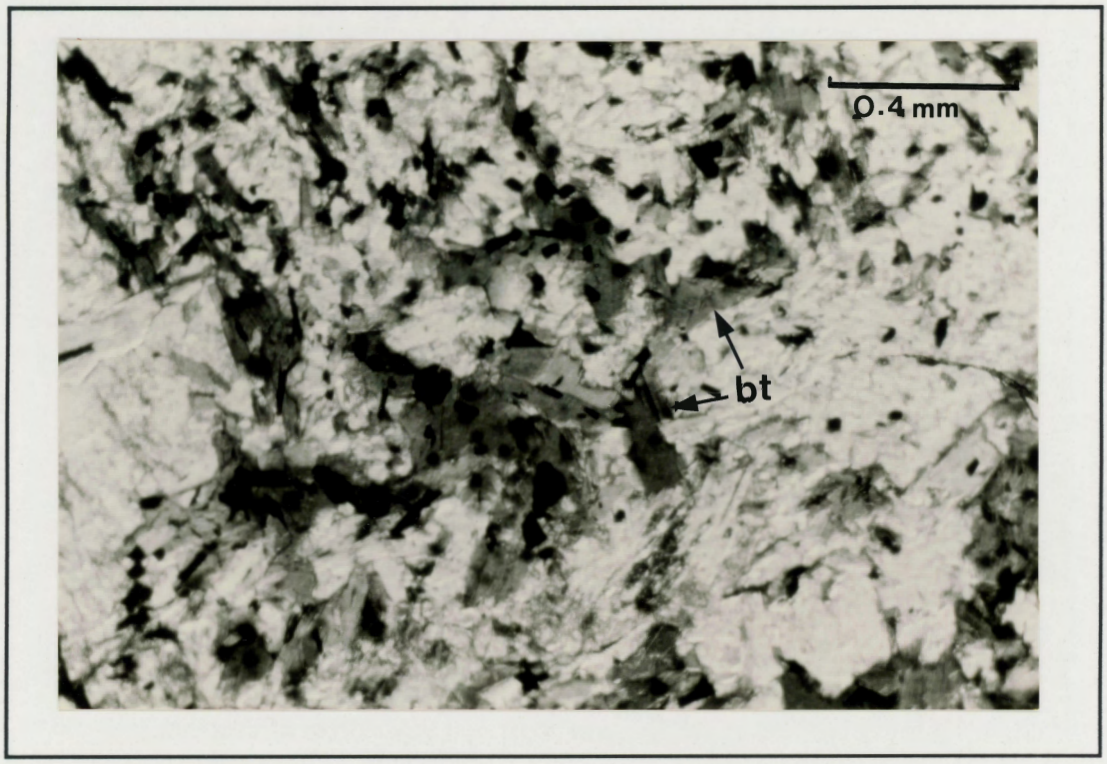

Figure 3.22. TML-3B. Early biotite shows extensive resorption with oxides.

fibrolite (Fig. 3.19), or resorbed against plagioclase and/or garnet (Fig. 3.22). Figure 3.23 shows secondary idiomorphic biotite which commonly occurs with embayed biotite. Inclusions of biotite in relict garnet are xenoblastic to sub-idioblastic and free of alteration or reaction to fibrolite or sillimanite. However, embayment of some biotite and minor replacement by fibrolite (Figs. 3.19 and 3.20) is apparent in the matrix.

Table 3.7 lists microprobe analyses of biotite inclusions in G1A, G1B, and G2A. The Fe/(Fe+Mg) ratio is lower (0.46-0.47) for G1A and G1B biotite inclusions than for inclusions in G2A (0.52-0.56) and for matrix biotite (0.47-0.51). As well, titanium is lower (0.92 and 0.97 weight percent) for G1A and G1B than for G2A inclusions (1.77 to 2.31 weight percent) and matrix biotite (1.44 to 2.53 weight percent). Manganese is undetectable in G1A and G1B biotite, and higher in G2A inclusions (0.28 to 0.32 weight percent) than matrix biotite (0.16 to 0.23 weight percent). Magnesium is slightly higher for the G1A and G1B (11.35 to 11.86 weight percent) than for other biotite (8.83 to 11.33 weight percent). These differences may be attributed to localized differences in bulk composition.

Muscovite

Muscovite in TML-6B is idioblastic and shows little replacement by fibrolite in contrast to TML-3B muscovite which is more extensively replaced by fibrolite. Muscovite composition (Table 3.8) shows approximately equal proportions of iron to magnesium. Iron and magnesium are significantly higher for xenoblastic muscovite in the TML-3B enclave (0.251 and 0.278 cations for 22 oxygens) than for idioblastic muscovite in the TML-6B enclave, shown in Figure 3.24 (0.101-0.118 and 0.093-0.121 cations for 22 oxygen), in contrast to sodium which is depleted in TML-3B (0.066 cations for 22 oxygen) relative to TML-6B (0.124-0.263 cations for 22 oxygen). Figure 3.25 shows relict staurolite enclosed in late idioblastic muscovite.

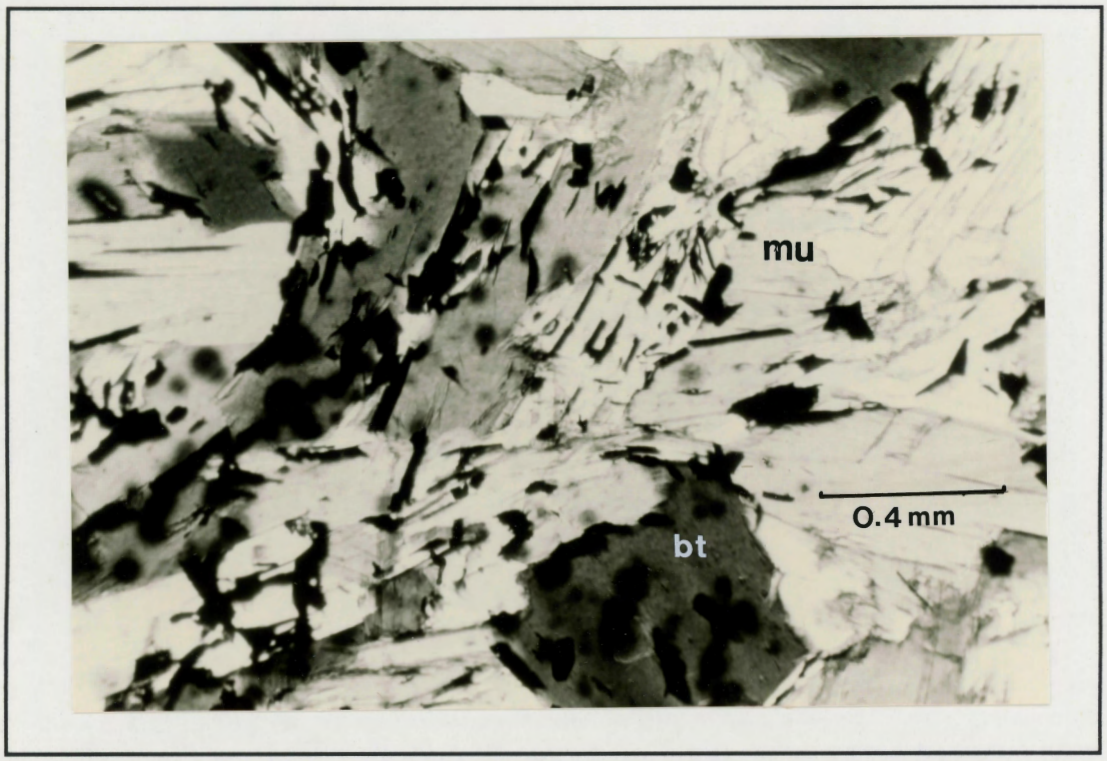

Figure 3.23. TML-6B. Secondary muscovite associated with slightly embayed biotite and Fe-Ti oxides.

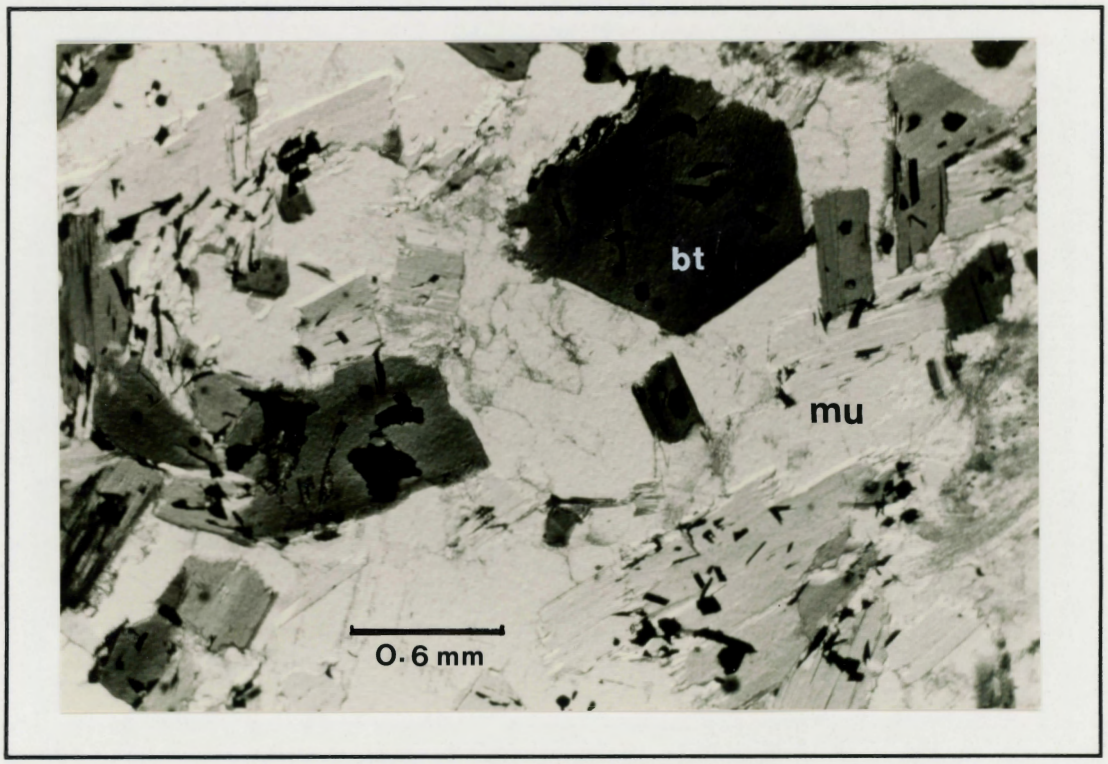

Figure 3.24. TML-6B. Late unaltered idioblastic biotite with muscovite and oxides.

TABLE 3.7. Microprobe analyses of biotite

	1[a]	2[b]	3[c]	4[c]	5[c]	6[d]	7[d]	8[d]	9[d]	10[d]	11[d]
SiO_2	35.80	35.38	34.87	35.04	33.36	35.98	35.10	35.79	36.28	35.86	35.62
TiO_2	0.92	0.97	2.31	1.77	1.81	2.06	1.72	1.44	2.53	2.48	1.52
Al_2O_3	19.52	20.71	18.31	18.70	19.74	19.90	18.66	19.66	18.88	19.93	19.37
FeO	18.14	18.17	19.44	19.89	19.76	18.32	18.63	18.69	18.43	17.95	18.22
MnO	0.00	0.00	0.32	0.30	0.28	0.21	0.17	0.23	0.19	0.16	0.18
MgO	11.86	11.35	8.54	10.17	8.83	9.77	10.23	10.32	9.94	10.65	11.33
CaO	0.00	0.00	0.11	0.02	0.00	0.02	0.02	0.00	0.01	0.04	0.02
Na_2O	0.04	0.21	0.09	0.09	0.07	0.06	0.11	0.06	0.19	0.25	0.19
K_2O	9.34	8.85	9.47	9.68	9.39	9.69	9.05	9.39	8.85	9.02	8.73
Total	95.62	95.64	94.46	95.66	96.01	93.24	93.69	95.58	95.30	95.34	95.18
					Cations per formula based on 22 oxygens						
Si	5.381	5.302	5.379	5.347	5.229	5.399	5.412	5.401	5.466	5.403	5.373
Al^{IV}	2.619	2.698	2.621	2.653	2.771	2.601	2.588	2.599	2.534	2.597	2.627
Al^{VI}	0.837	0.956	0.705	0.708	0.873	0.917	0.801	0.895	0.816	0.762	0.814
Ti	0.105	0.110	0.271	0.205	0.216	0.235	0.201	0.165	0.290	0.284	0.174
Fe	2.280	2.277	2.508	2.538	2.590	2.299	2.402	2.359	2.322	2.262	2.298
Mn	0.000	0.000	0.042	0.039	0.037	0.027	0.022	0.029	0.024	0.020	0.023
Mg	2.657	2.535	2.193	2.313	2.063	2.185	2.351	2.321	2.232	2.391	2.547
Ca	0.000	0.000	0.018	0.003	0.000	0.003	0.003	0.000	0.002	0.006	0.003
Na	0.012	0.061	0.027	0.027	0.021	0.017	0.033	0.018	0.056	0.073	0.056
K	1.791	1.692	1.854	1.885	1.878	1.885	1.780	1.808	1.701	1.734	1.680
Fe/(Fe+Mg)	0.46	0.47	0.53	0.52	0.56	0.51	0.51	0.50	0.51	0.49	0.47
Mg/(Fe+Mg)	0.54	0.53	0.47	0.48	0.44	0.49	0.49	0.50	0.49	0.51	0.53

a: core inclusion in G1A
b: core inclusion in G1B
c: inclusions in G2A
d: matrix biotite

TABLE 3.8. Microprobe analyses of muscovite.

	1[a]	2[b]	3[b*]	4[b]	5[b]
SiO_2	49.60	51.56	47.94	47.94	45.43
TiO_2	0.00	0.55	0.13	0.91	0.89
Al_2O_3	33.47	35.99	37.38	34.26	34.70
FeO	2.03	1.00	0.93	1.01	1.03
MnO	0.00	0.00	0.00	0.00	0.00
MgO	1.43	0.56	0.48	0.61	0.54
CaO	0.00	0.00	0.00	0.00	0.00
Na_2O	0.26	0.95	1.05	0.48	0.78
K_2O	9.22	7.44	8.49	8.73	7.55
Total	96.28	98.05	96.40	93.94	90.92
Cations per formula based on 22 oxygens					
Si	6.473	6.484	6.200	6.367	6.215
Al^{IV}	1.527	1.516	1.800	1.633	1.785
Al^{VI}	3.617	3.815	3.894	3.727	3.806
Ti	0.000	0.053	0.013	0.092	0.093
Fe	0.251	0.105	0.101	0.112	0.118
Mn	0.000	0.000	0.000	0.000	0.000
Mg	0.278	0.105	0.093	0.121	0.110
Ca	0.000	0.000	0.000	0.000	0.000
Na	0.066	0.232	0.263	0.124	0.207
K	1.535	1.194	1.401	1.479	1.318
Fe/(Fe+Mg)	0.47	0.50	0.52	0.48	0.52
Mg/(Fe+Mg)	0.53	0.50	0.48	0.52	0.48

a: TML-3B; xenoblastic muscovite

b: TML-6B; idioblastic muscovite

* muscovite rimming staurolite in Figure 3.26

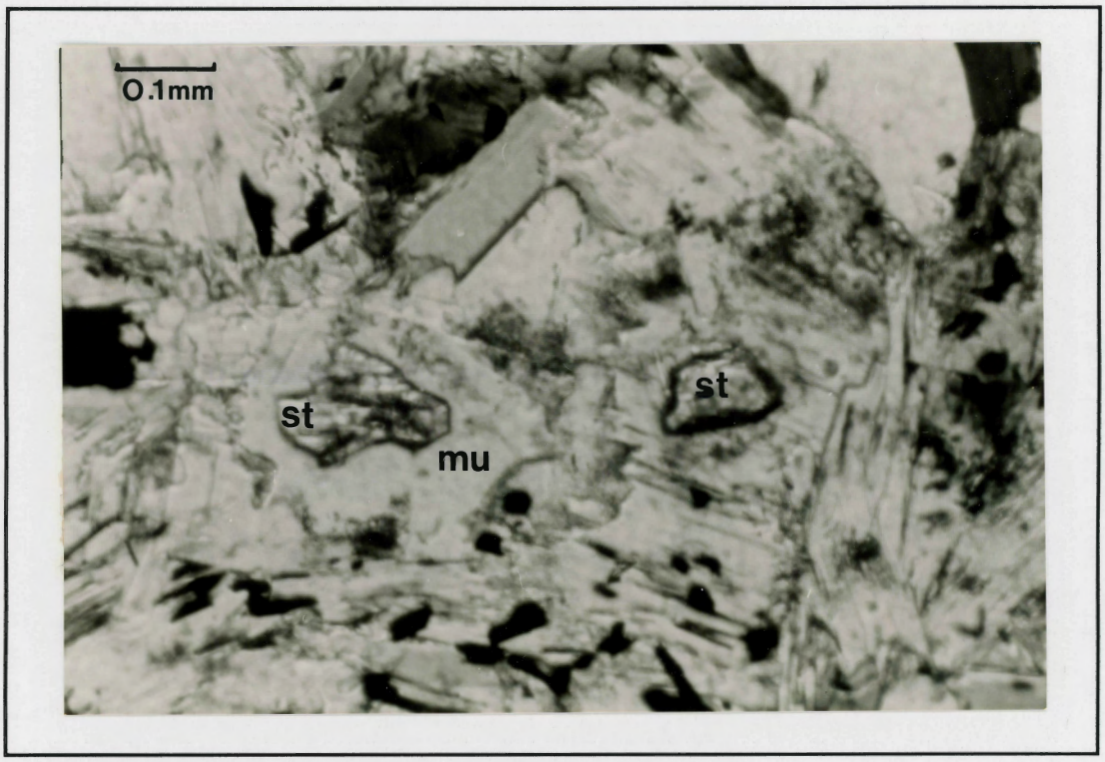

Figure 3.25. TML-6B. Relict staurolite in secondary muscovite.

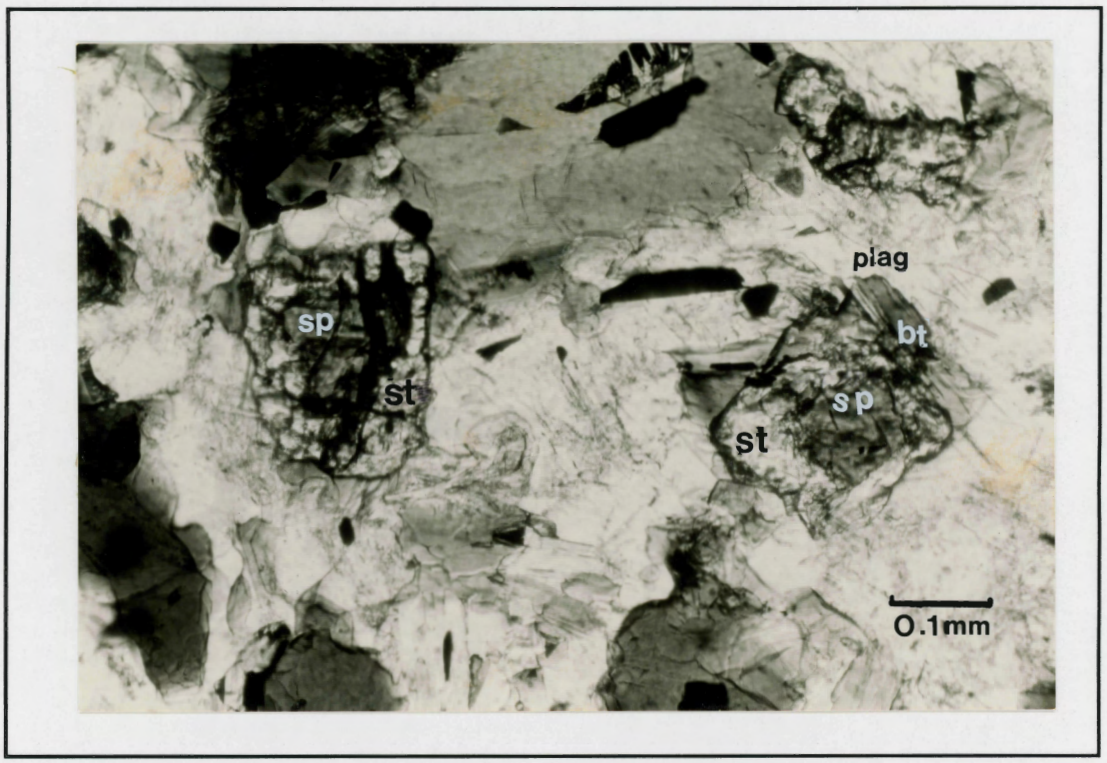

Figure 3.26. TML-8D. Zincian hercynite with hematite inclusions rimmed with resorbed zincian staurolite with magnetite inclusions against resorbed biotite and plagioclase.

Idioblastic secondary and minor xenoblastic muscovite locally shows evidence for the reaction to produce fibrolite, but little for the production of K-feldspar by the equation,

$$\text{muscovite} + \text{quartz} \rightleftharpoons \text{sillimanite} + \text{K-feldspar} + H_2O.$$

The nucleation of fibrolite in muscovite appears to have resulted from the polymorphic inversion of sillimanite and kyanite to fibrolite without the use of muscovite as a catalyst (Carmichael, 1969).

Spinel and staurolite

Green spinel (Fig. 3.26) is observed in pelitic enclaves adjacent to zoned calc-silicate inclusions. The zincian hercynite, having a typical chemical formula of $(Fe_{0.5}Zn_{0.4}Mg_{0.1})Al_2O_4$ (Table 3.9), is entirely rimmed by staurolite (Table 3.9) containing quartz inclusions which is resorbed against biotite and plagioclase. Staurolite also occurs independently as a relict phase partly to entirely replaced by plagioclase, muscovite, and biotite.

The reaction between zincian hercynite and staurolite proceeds via a reaction involving biotite, iron oxides, aluminum silicates, water, oxygen, and quartz, as in the following balanced reaction, based on mineral assemblages and mineral chemistry of the Ten Mile Lake enclaves,

$$\underset{\textit{zincian hercynite}}{100\ (Fe_{.48}Zn_{.38}Mg_{.11}Al_{.02})Al_2O_4} + \underset{\textit{biotite}}{42\ K_2(Fe_{1.27}Mg_{1.15}Al_{.35})(Si_{2.67}Al_{1.33})O_{10}(OH)_2}$$

$$+ \underset{\textit{hematite}}{250\ Fe_2O_3} + \underset{\textit{aluminum silicate}}{1135\ Al_2SiO_5} + \underset{\textit{water}}{282\ H_2O}$$

$$\rightleftharpoons$$

$$\underset{\textit{staurolite}}{240\ (Fe_{1.26}Mg_{.23}Zn_{.16}Al_{.07})Al_9O_6(Si_{3.47}Al_{.53})O_{16}(OH)_2} + \underset{\textit{magnetite}}{100\ Fe_3O_4} + \underset{\textit{oxygen}}{68\ O_2}.$$

$$+ \underset{\textit{muscovite}}{84\ K(Fe_{.05}Mg_{.05}Al_{1.95})(Si_{3.1}Al_{.9})O_{10}(OH)_2} + \underset{\textit{quartz}}{154\ SiO_2}$$

TABLE 3.9. Microprobe analyses of zincian hercynite and staurolite in the TML-8D xenolith

	1[a]	2[a]	3[a]	4[b]	5[b]	6[b]
SiO_2	0.00	0.00	0.00	32.49	24.77	25.66
Al_2O_3	59.31	58.77	58.47	54.73	58.11	26.12
FeO	19.70	21.22	21.51	9.99	10.77	10.74
MgO	2.57	2.84	2.85	1.29	1.09	1.20
ZnO	17.95	15.92	16.23	1.30	1.58	1.41
Total	99.53	98.75	99.06	99.80	96.32	95.13
			Cations per formula			
Si	0.00	0.00	0.00	4.319	3.472	3.635
Al	2.018	2.011	2.002	8.570	9.592	9.362
Fe	0.476	0.516	0.523	1.111	1.262	1.272
Mg	0.111	0.123	0.123	0.256	0.228	0.253
Zn	0.383	0.342	0.348	0.128	0.164	0.147

a: zincian hercynite; cation on the basis of 4 oxygens

b: zincian staurolite; cations on the basis of 24 oxygens

The biotite composition is based on an analysis of inclusions in garnet G2A (Table 3.7 4^b) which may be characteristic of pre-entrainment biotite consumed during the reaction. Both garnet G2A and zincian hercynite are found in more mafic enclaves. The formula for muscovite is based on analysis 3^b (Table 3.8) of muscovite enveloping relict staurolite, shown in Figure 3.25. The reaction is consistent with petrographic observations of hematite inclusions in zincian spinel rimmed with staurolite containing inclusions of magnetite and quartz (Fig. 3.26). Aluminum silicate minerals are abundant in the enclaves, as is water from dehydration reactions and the calc-silicate, transferred by diffusion between grains and along microfractures.

Zincian hercynite is reported to rim staurolite through progressive metamorphism and the dehydration of staurolite (Schumacher 1985; Stoddard 1979; Atkin 1978). In these enclaves staurolite rims zincian hercynite and, therefore, suggests retrograde metamorphism.

Summary

The mineral assemblages observed in the pelitic enclaves are summarized in Table 3.1. The pre-entrainment phases typically indicate a higher pressure and temperature (kyanite, sillimanite, and zincian hercynite) than the other metamorphic assemblages. The relict phases are xenoblastic exhibiting non-equilibrium with respect to the matrix.

Late fibrolite pseudomorphs, late biotite, and muscovite are generally associated with syn-entrainment metamorphism. Abundant fibrolite, common in contact metamorphism, suggest that the syn-entrainment metamorphism was controlled by rapid cooling of the host felsic intrusion.

Table 3.10. Summary of mineralogy and mineral chemistry.

Pre-entrainment	Syn-entrainment
Garnets	
Mn-poor, resorbed, up to 2 mm with inclusions of biotite, quartz, and Fe-Ti oxides. Complex chemical zonation. **(G1A)**	Mn-poor, idioblastic, up to 3mm with inclusions of biotite, quartz, and Fe-Ti oxides. Mn increasing toward the rims. **(G1B)**
Mn-rich, subidioblastic to idioblastic, up to 3 mm with inclusions of biotite, quartz, plagioclase, fibrolite, and Fe-Ti oxides. Complex chemical zonation. **(G2A)**	Mn-rich, idioblastic , up to 300 μm with inclusions of quartz. Mn and Fe increasing toward the rims. **(G2B)**
Matrix minerals	
kyanite and sillimanite with reaction rims	fibrolite
biotite	biotite
plagioclase; An 30 core to An 25 for original rim	plagioclase; An 24 cores to An 41 rims
staurolite rimmed with secondary muscovite	muscovite
zincian hercynite with rims of staurolite	

CHAPTER 4: GEOTHERMOMETRY AND GEOBAROMETRY

4.1 Thermometry and Barometry Calculations

4.1.1 Garnet - Biotite Thermometers

Temperature estimates for the Ten Mile Lake xenoliths are determined using garnet - biotite pairs and PTLEO (Nadeau, *unpubl.*), a thermobarometry software package which estimates temperature based on calibration of the garnet - biotite equilibrium (Thompson 1976; Ferry and Spear 1978; Ganguly and Saxena 1984; Indares and Martignole 1985). The garnet - biotite thermometer is based on the temperature-dependent cationic exchange of Fe and Mg between end member components of garnet and biotite by the reaction,

$$\underset{\textit{almandine}}{Fe_3Al_2Si_3O_{12}} + \underset{\textit{phlogopite}}{KMg_3AlSi_3O_{10}(OH)_2} \rightleftharpoons \underset{\textit{pyrope}}{Mg_3Al_2Si_3O_{12}} + \underset{\textit{annite}}{KFe_3AlSi_3O_{10}(OH)_2}$$

The thermometry equations, given in Table 4.1, are based on experimental or empirical determination of entropy, enthalpy, and free energy of the reaction for the cation exchange between garnet and biotite and require only the Fe - Mg distribution coefficient (K_D) of the two minerals and an estimate of pressure. The Fe - Mg distribution coefficient is calculated from microprobe analyses. Although a pressure estimate is required, the change in temperature resulting from varying pressure by up to 5 kb is still within the error of the calibration. An estimate of pressure based on mineral assemblage is usually sufficient. The thermometers are generally considered to have an accuracy of $\pm$ 50 °C as determined from the propagation of uncertainties in entropy, enthalpy, and free energy through the equations, although some authors claim considerably smaller associated errors (Essene 1989; Hodges and Crowley 1985). These are

Table 4.1. Thermometers and barometers used in temperature and pressure estimates.

Equation	Source
$2740 - 1.56\,T\,(^{o}K) + 0.0.24\,P(bar) + 6\,T\,(^{o}K)\ln K_D = 0$	Thompson (1976)
$12{,}454 - 4.662T\,(^{o}K) + 0.057P\,(bars) + 3RT\ln K_D = 0$	Ferry and Spear (1978)
$\ln K_D T(^{o}K) + 0.782\,T(^{o}K) =$ $A+0.503\,[W_{Fe\text{-}Mg}(X_{Fe}-X_{Mg}) + \Delta W_{Ca}X_{Ca} + \Delta W_{Mn}X_{Mn}]^{gt}$ where $A= 2089-2.48W^{gt}_{Fe\text{-}Mg}+ 9.45P(Kb)$ at $X_{Ca}^{gt} \leq 0.30$ and $X_{Mn}^{gt} \leq 0.30$ $\Delta W_{Ca} = W_{Mg\text{-}Ca} - W_{Fe\text{-}Ca} = 3{,}000 \pm 500$ cal/ mole of cation $\Delta W_{Mn} = W_{Mg\text{-}Mn} - W_{Fe\text{-}Mn} = 3{,}000 \pm 500$ cal/ mole of cation $W^{gt}_{Fe\text{-}Mg}=200\,[Mg/(Mg+Fe)]^{gt}+2500\,[Fe/(Mg+Fe)]^{gt}$	Ganguly and Saxena (1984)
$(176-3448P)/T + 8.3969 + \log (a_{gr}/a_{an})^3 + \log (\gamma_{gr}/\gamma_{an})^3 = 0$	Ghent *et al.* (1979)
$\Delta V\,P\,(bars) = 2.333-0.2578\,T\,(^{o}C) - 1.396\,T\,(^{o}K)\ln (a_{gr}/a_{an})^3$ when sillimanite is the stable aluminum silicate, and ΔV= partial volume change at 1 bar $= [V_{gr}+V_{sill}+V_{qz}]-[V_{an}]$	Newton and Haselton (1981)

where $K_D= (Mg/Fe)^{gt}/Mg/Fe)^{bt}$, for 1,2 and 4; $K_D= (Mg/Fe)^{gt}/Mg/Fe)^{bt}$, for 3; γ_{gr} = activity of grossular; γ_{an} = activity of anorthite

$X_i bt = i / (Fe + Mg + Mn + Al^{VI} + Ti)$ for i = Al and Ti

$X_i gt = i / (Fe + Mg + Mn + Ca)$ for i = Mn and Ca

$a_{gr}=\gamma_{gr}X_{gr}$ $W_{Ca\text{-}Mg}= 3300 - 1.5\,T(^{o}K)$,

$\ln \gamma_{gr}= [W_{Ca\text{-}Mg}(X_{py}+X_{py}X_{alm})]/ 1.987T(^{o}K)$,

$a_{an}= \frac{X_{an}(1+X_{an})^2}{4} \exp \{\frac{(1+X_{an})^2(2050 + 9392X_{an})}{RT}\}$

minimum errors and do not include analytical errors incurred from microprobe analyses. However, most uncertainty is a result of uncertainties in entropy and enthalpy and only a very small part of the cumulative uncertainty is a result of analytical errors in microprobe analyses (Hodges and Crowley 1985).

Thompson (1976) and Ferry and Spear (1978) assume that both garnet and biotite are ideal solutions with respect to Fe-Mg exchange. However, the Ganguly and Saxena (1984) thermometer considers the effects of Mn and Ca in garnet on the distribution coefficient of Fe and Mg between garnet and biotite. Increasing Ca and Mn, especially for $X_{Ca} \geq 0.30$ (X_X defined in Table 4.1), causes a decrease in the K_D and thus increases the temperature estimate.

Indares and Martignole (1985) suggest a correction for Ti and Al in the 6-fold site for biotite with $X_{TiAl} > 0.20$, which is dependent on the ratio of Mn/Mg.

4.1.2 Garnet - Plagioclase - Al_2SiO_5 - Quartz Barometers

Pressure estimates are based on the pressure-dependent continuous distribution of Ca between anorthite and grossular in the presence of aluminum silicate and quartz by the reaction,

$$\underset{\textit{anorthite}}{3\ CaAl_2Si_2O_8} \rightleftharpoons \underset{\textit{grossular}}{Ca_3Al_2Si_3O_{12}} + \underset{\textit{ky/sill/and}}{2\ Al_2SiO_5} + \underset{\textit{quartz}}{SiO_2}.$$

This barometer is normally used in conjunction with the garnet - biotite thermometer to calculate pressure and temperature simultaneously. The equations derived from Ghent *et al.* (1979) and Newton and Haselton (1981) (Table 4.1), and Ca and Mn corrections of Ganguly and Saxena (1984) applied to standard equations of Ghent *et al.* (1979) and Newton and Haselton (1981) are used to calculate pressure. This barometer is generally restricted to garnets with Mn < 1/3 Mg and has an accuracy within ± 1.5 Kb.

4.2 Data

4.2.1 Representative Microprobe Analyses and Their P-T Estimates

Pressure estimates are calculated from low Mn garnets with core inclusions of biotite which are both xenoblastic and idioblastic (Figs. 4.1a and 4.1b). No

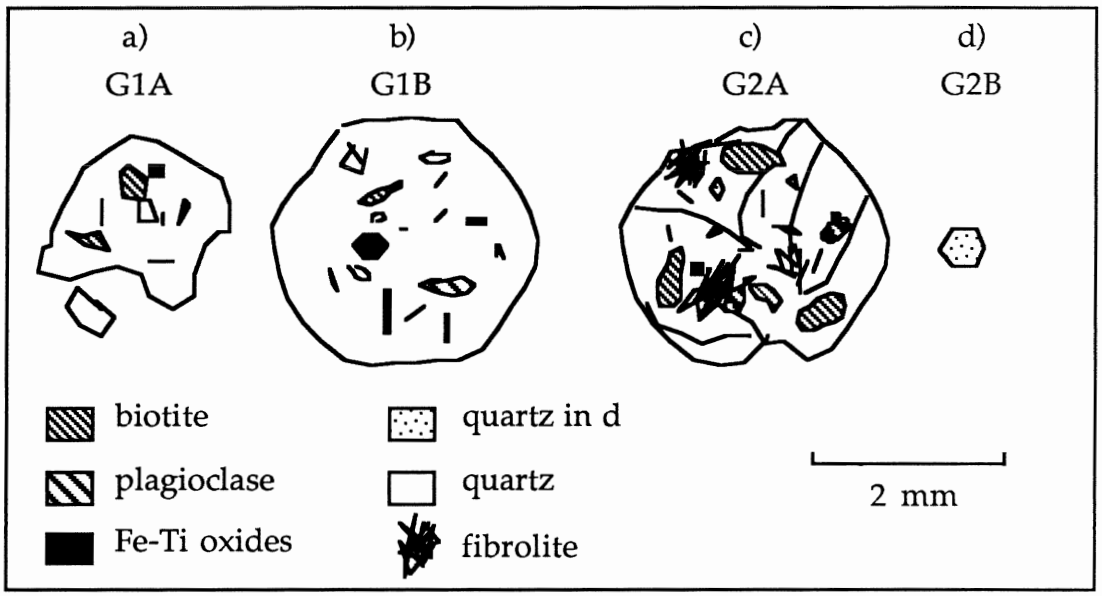

Figure 4.1 Sketch of the pelitic garnets and their inclusions for thermobarometry. Pressure and temperature relations as determined from a) G1A: a low Mn, xenoblastic garnet with inclusions of bt (+ quartz and Fe-Ti oxides), b) G1B: a low Mn, idioblastic garnet with inclusions of bt (+ quartz and Fe-Ti oxides), c) G2A: a high Mn, sub-idioblastic garnet with inclusions of bt-pl-qt-Al_2SiO_5 (+ Fe-Ti oxides), d) G2B: a high Mn, idioblastic garnet and matrix assemblage bt-pl-qt-Al_2SiO_5

Al_2SiO_5 or plagioclase is present as inclusions in these garnets, therefore no pressure can be calculated for the Mn-poor garnets. Large Mn-rich garnets (Fig. 4.1c) and their inclusions of plagioclase, fibrolite, and quartz are used to determine both temperature and pressures at early stage of metamorphism (garnet cores). Small garnets (Fig. 4.1d) and matrix plagioclase, fibrolite, quartz yield both pressures and temperatures of the final stage of metamorphism. Temperature calculations using the Indares and Martignole (1985) correction for excess Al and Ti are not necessary, as the $X_{Al}{}^{bt}$ and $X_{Ti}{}^{bt}$ (as defined in Table 4.1), do not exceed the maximum recommended value of < 0.20. Garnet $X_{Mn}{}^{gt}$ and $X_{Ca}{}^{gt}$ are well below the levels at which excess Ca and Mn affects K_D. Barometers with corrections for Ca and Mn are likely to be less accurate for these garnets in the light of low concentrations of Ca and Mn, and therefore were not applied.

TABLE 4.2. Representative microprobe analyses of garnet, biotite, and plagioclase for thermobarometry estimates given in Table 4.3.

	G1A		G1B		G2A			G2B		
	1a-g	2a-b	3a-g	4a-b	5b-g	6b-b	7b-p	8c-g	9c-b	10c-p
SiO_2	37.25	34.69	36.95	35.38	37.05	33.36	61.63	36.73	35.21	62.29
TiO_2	0.12	2.48	0.07	0.97	0.04	1.81	0.00	0.06	1.48	0.00
Al_2O_3	20.88	17.97	21.77	20.71	21.69	19.74	24.32	20.69	19.24	24.53
Cr_2O_3	0.06	0.03	0.00	0.00	0.02	0.04	0.00	0.12	0.02	0.00
FeO	34.03	21.09	35.20	18.17	30.00	19.76	0.33	30.49	18.61	0.22
MnO	1.53	0.22	1.23	0.00	7.05	0.28	0.00	8.52	0.20	0.00
MgO	4.92	10.43	4.08	11.35	3.53	8.83	0.00	2.13	9.76	0.00
CaO	1.10	0.12	1.03	0.00	1.13	0.00	5.43	1.31	0.02	5.49
Na_2O	0.00	0.15	0.00	0.21	0.00	0.07	8.78	0.00	0.10	8.11
K_2O	0.00	7.89	0.00	8.85	0.00	9.39	0.00	0.00	8.91	0.00
Total	99.89	95.07	100.33	95.64	100.51	93.28	100.49	100.05	93.55	100.64
					Cations per formula					
Si	5.962	5.315	5.905	5.302	5.925	5.229	10.904	5.973	5.426	10.959
Ti	0.038	0.289	0.008	0.110	0.005	0.105	0.000	0.007	0.173	0.000
Al^{IV}	3.898	2.685	0.095	2.698	0.075	2.771	1.096	0.027	2.574	1.041
Al^{VI}	0.015	0.557	4.003	0.956	4.010	0.873	3.972	3.936	0.917	4.042
Cr	0.008	0.000	0.000	0.000	0.003	0.000	0.000	0.015	0.000	0.000
Fe	4.555	2.702	4.705	2.277	4.012	2.590	0.048	4.147	2.398	0.032
Mn	0.207	0.029	0.167	0.000	0.955	0.037	0.000	1.174	0.026	0.000
Mg	1.174	2.381	0.972	2.535	0.841	2.063	0.000	0.516	2.241	0.000
Ca	0.189	0.020	0.176	0.000	0.194	0.000	1.026	0.228	0.003	1.035
Na	0.000	0.045	0.000	0.061	0.000	0.021	3.012	0.000	0.030	2.767
K	0.000	1.542	0.000	1.692	0.000	1.878	0.000	0.000	1.752	0.000
Fe/(Fe+Mg)	0.80	0.53	0.83	0.47	0.83	0.56		0.89	0.52	
Mg/(Fe+Mg)	0.20	0.47	0.17	0.53	0.17	0.44		0.11	0.48	
$Al^{VI}/(Al^{VI}+Ti+Fe+Mg)$		0.09		0.16		0.16			0.16	
$Ti/(Al^{VI}+Ti+Fe+Mg)$		0.05		0.02		0.02			0.03	
Alm	0.744		0.782		0.668			0.684		
Gr	0.034		0.029		0.032			0.038		
Py	0.192		0.161		0.140			0.085		
Sp	0.031		0.028		0.159			0.194		
Mn/(Ca+Mn+Fe+Mg)	0.03		0.03		0.16			0.19		
Ca/(Ca+Mn+Fe+Mg)	0.03		0.03		0.03			0.04		
Alm/Py	3.88		4.84		4.77			8.05		

a: TML-8C
b: TML-4B
c: TML-3B

g: garnet; cations per formula based on 24 oxygens
b: biotite; cations per formula based on 24 oxygens
p: plagioclase; cations per formula based on 32 oxygens

TABLE 4.3. Summary of pressure and temperature estimates from typical microprobe analyses given in Table 4.2. (1 to 4 give temperatures for 2 to 8 kb)

Thermometer or barometer	G1A T(C)	G1B T(C)	G2A T(C)	G2A P(kb)	G2B T(C)	G2B P(kb)
1	712	574	677		495	
2	775-803	582-605	723-750		480-501	
3	763-791	589-612	774-801		551-571	
4			740	5.7	482	2.3
5			714	5.5	474	1.5

1: Thompson (1976)
2: Ferry and Spear (1978)
3: Ganguly and Saxena (1984)
4: Ghent et al. (1979)
5: Newton and Haselton (1981)

Calculations based on microprobe analyses of biotite inclusions in the low Mn, xenoblastic G1A (Table 4.2) range from 712 to 803 °C with an average of 755 ± 50 °C. A core inclusion of biotite in G1B gives temperatures between 574 °C and 612 °C for the three thermometers (Table 4.3). An average estimate of 595 ± 50 °C is calculated from biotite - garnet thermometers. Microprobe analyses of inclusions of biotite and plagioclase in G2A (Table 4.2) produce average pressure and temperature estimates (Table 4.3) of 740 ± 50 °C and 5.6 ± 1.5 Kb. Thermobarometry calculations from microprobe analyses of G2B garnets with matrix biotite and plagioclase are given in Table 4.2 with pressure - temperature estimates in Table 4.3.

The Fe/(Fe + Mg) ratio for each garnet is at the lower end of the suggested range of 0.80-1.00. Also, the almandine to pyrope ratios for the garnets range from 4.77 to 8.05, and are all above the suggested level of 3.0.

4.2.2 Summary of Pressure and Temperature Estimates

Table 4.4 lists pressure and temperature estimates for each garnet population. Higher temperatures are determined for G1A and G2A at 755 ± 50° C and 740 ± 50° C, respectively. Temperatures of 595 ± 50° C and 525 ± 50° C are calculated for

Table 4.4. Summary of pressure and temperature estimates (columns # 1 to 5 correspond to thermometers and barometers listed below).

Xenolith	Garnet	1 T(°C)	2 T(°C)	3 T(°C)	4 T(°C)	4 P(Kb)	5 T(°C)	5 P(Kb)
TML-4B*	G1A	753	836-866	811-841				
TML-4B•	G1A	805	916-949	819-851				
TML-8C°	G1A	712	775-803	763-791				
TML-3B°	G1B	613	635-659	686-711				
TML-8C*	G1B	583	594-618	618-642				
TML-8C‡	G1B	574	582-605	589-612				
TML-3B•	G2A	619	642-667	701-725				
TML-4B•	G2A	641	673-699	737-762				
TML-4B*	G2A	519	510-531	591-612	514	3.1	503	2.9
TML-4B‡	G2A	677	723-750	774-801	740	5.7	714	5.5
TML-8B*	G2A	582	592-616	650-674	599	3.6	585	3.5
TML-8B*	G2A	557	559-582	612-634	562	2.7	551	2.7
TML-3B*	G2B	578	587-610	640-663	583	1.1	579	1.1
TML-3B*	G2B	498	484-504	553-573	483	1.8	477	1.8
TML-3B*	G2B	498	484-504	553-573	483	1.9	477	1.9
TML-3B*	G2B	493	477-498	546-567	476	1.7	471	1.7
TML-3B*	G2B	572	579-602	631-654	575	1.0	571	1.0
TML-3B*	G2B	572	579-602	631-654	575	1.0	571	1.0
TML-3B*	G2B	578	587-610	640-663	583	1.1	579	1.2
TML-3B*	G2B	507	495-516	564-585	496	2.5	488	2.5
TML-3B*	G2B	506	494-515	560-580	492	1.5	487	1.5
TML-3B*‡	G2B	495	480-501	551-571	482	2.3	474	2.4
TML-3B*	G2B	549	549-572	614-636	555	3.4	542	3.5
TML-3B*	G2B	517	508-529	576-597	509	2.5	501	2.6
TML-8B*	G2B	546	545-567	605-627				
TML-8C*	G2B	533	528-550	583-605				
TML-8C*	G2B	562	565-588	616-638				

1: Thompson (1976)
2: Ferry and Spear (1978)
3: Ganguly and Saxena (1984)
4: Ghent et al. (1979)
5: Newton and Haselton (1981)

‡ microprobe analyses fond in Table 4.2
*rim of garnet with matrix biotite
° core analyses
• intermediate rim to core
columns # 1 to 3 give temperatures for 2 to 8 kb

G1B and G2B. The pressure calculation for an inclusion intermediate between the core and rim of G2B is 5.6 ± 1.5 kb. The numerous calculations for G2B suggest a pressure of 2.3 ± 1.5 kb.

4.3 Pressure, Temperature, and Time

The pressure and temperature conditions of the Ten Mile Lake enclaves are summarized in Table 4.5. The relict garnets yield similar temperature estimates (755 °C and 740 °C), as do the the idioblastic garnets (595 °C and 525 °C), within the 50 °C error for each. Pressures could not be obtained for the Mn-poor garnets owing to the lack of plagioclase and aluminum silicate inclusions in the garnets.

The data show that relict G2A has rim temperatures similar to G1A and G2B; however, relict G1B does not. This preservation of high temperature composition is consistent with its more corroded nature than the high Mn relict garnets, G2A. Therefore, the garnets have recorded at least two stages of metamorphism. The pressure - temperature path, illustrated in Figure 4.2, suggest that both Mn-rich and Mn-poor corroded garnets grew at a similar temperatures and possibly pressures. Likewise, the idioblastic Mn-rich and Mn-poor garnets grew at similar temperatures, but lower than those estimated from corroded garnets by approximately 200 °C. Without pressure estimates for the Mn-poor garnets, it is difficult to test whether the difference in bulk garnet chemistry is a result of localized differences in bulk composition or fluctuations

Table 4.5. Pressure and Temperature estimates for the Ten Mile Lake enclaves.

Garnet	Pressure	Temperature	Mn	Nature of Garnet
G1A	undetermined	755 ± 50°C	low	xenoblastic
G1B	undetermined	595 ± 50°C	low	idioblastic
G2A	5.6 ± 1.5 Kb	740 ± 50°C	high	sub-idio to xenoblastic
G2B	2.3 ± 1.5Kb	525 ± 50°C	high	idioblastic

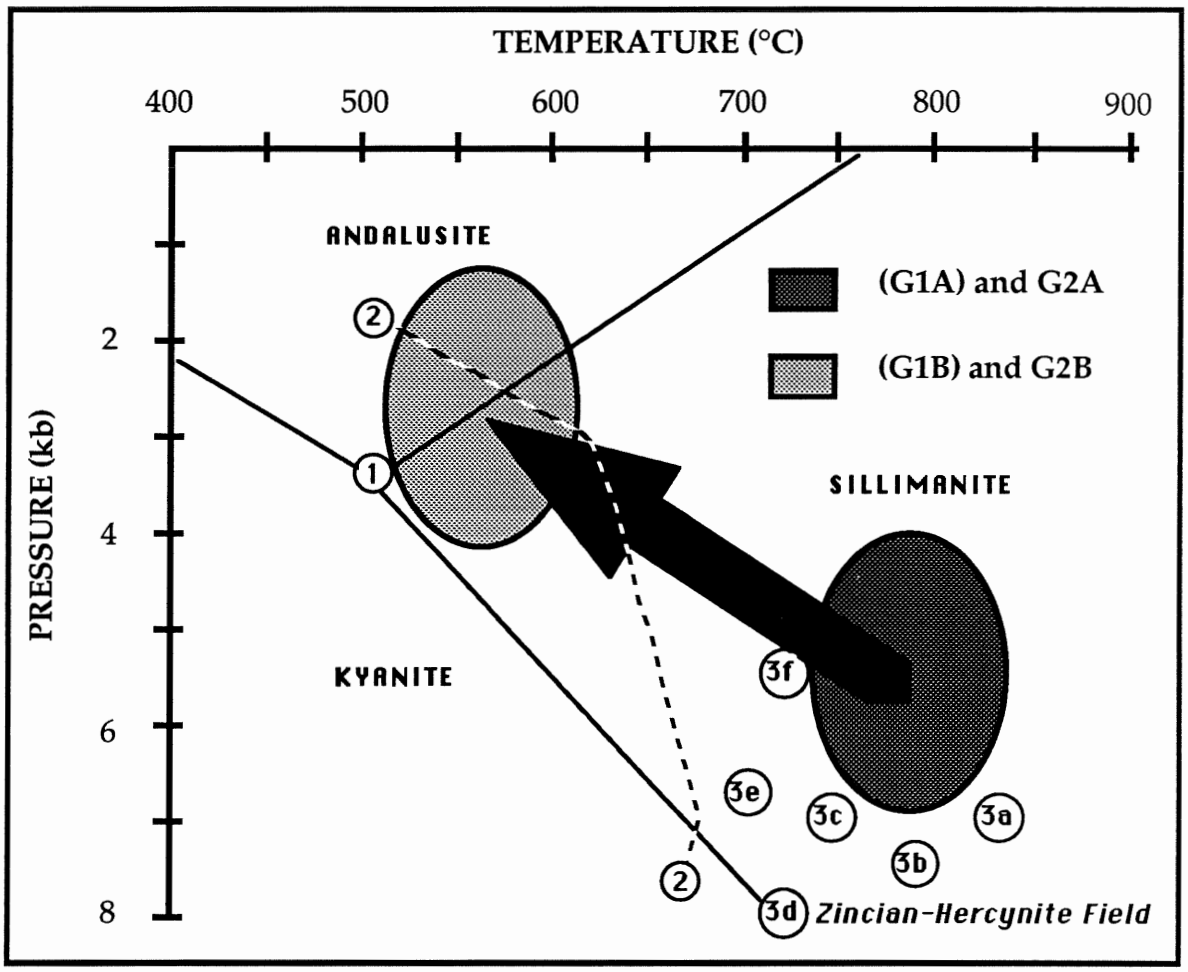

Figure 4.2 Pressure - Temperature Path. Pressure and temperatures are based on estimates of garnet - biotite - Al_2SiO_5 -plagioclase - quartz thermobarometry. Metamorphism 1: 780 ± 50 °C and 5.6 ± 1.5 Kb, Metamorphism 2: 560 ± 50°C and 2.3 ± 1.5 Kb. G1A and G2A are early Mn-poor and rich garnets. The pressure of G1A is inferred to be similar to G2A. G1B and G2B are late Mn-poor and rich garnets. The pressure of G1B is inferred to be similar to G2B. Data Sources for the curves and plots are as follows; **(1)** The aluminum silicate phase relations of Holdaway (1971); **(2)** Fe-staurolite + quartz (left) = Almandine + Al_2SiO_5 + H_2O (right) of Yardley (1981); **(3)** zincian-hercynite field compiled from Sculters and Bohlen (1989) where **a)** Zn = 3 %, **b)** Zn = 15 %, **c)** Zn = 31 %, **d)** Zn = 44 %, **e)** Zn = 48 %, and **f)** Zn = 57 %. In this study, zincian-hercynite contains 38 % Zn.

in temperatures and pressures. To simplify, the P-T path of Figure 4.2 assumes that Mn content is a function of bulk composition and that G1A and G2A are pre-entrainment Mn-poor and Mn-rich garnets whereas, G1B and G2B are syn-entrainment garnets.

CHAPTER 5: DISCUSSION

5.1 Origins of Zonation

Garnets

Normal zoning in garnets is associated with an increase of Fe and Mg and a decrease in Mn and Ca and generally indicates increasing grade of metamorphism, assuming no changes in bulk chemistry. The zonation of Fe, Mg, Ca, and Mn from the core to the rim in garnets (Fig. 3.13) is useful in the determination of the metamorphic history of a rock.

Four garnet populations are present throughout these pelitic enclaves and represent two stages of distinct pressure and temperature conditions. Pre-entrainment garnets, G1A and G2A, have higher P-T conditions associated with their inclusions and a complex reverse and normal zoning. The zonation in the garnet core is probably a result of changes in metamorphic grade in a closed system. The zonation at the rim may be influenced by the inclusion and disaggregation of the enclaves in the magma and cannot be assumed to be completely isochemical. Therefore, zonation from the core to the rims of the pelitic garnets probably became less a function of changes in metamorphic grade as changes in bulk chemistry become more important during entrainment.

The syn-entrainment garnets (G1B and G2B) show reverse zoning as indicated by an increase of Mn and a relative depletion in Mg. However, Fe increases with Mn. This reverse zoning may suggest either retrograde metamorphism or an influx of Fe. The extreme reverse zoning at the rims of G1B and G2B and the unusual increase of Fe with the depletion of Mg would suggest that the zonation is not purely an isochemical response to a decrease in metamorphic grade.

The Ca content of the garnets increases from pre- to syn-entrainment associations. Garnets in Mn-poor and Mn-rich portions of the enclaves have increased Ca content probably in response to a decreasing grade of metamorphism (Yardley, 1989). It is difficult to determine if changes in bulk chemistry, with respect to Ca, are associated with the entrainment of the pelitic enclaves in the host. It appears, however, that there has not been a loss of Ca to the host during entrainment.

Plagioclase

Assuming that plagioclase nucleates and grows in a closed system, normal zoning involves a decrease in Ca from core to rim in response to falling. Reverse zoning in rims of normally zoned plagioclase (Fig. 3.16) suggests either a temperature increase after a period of cooling or a later influx of Ca. If the increase in Ca at the rim of complexly zoned plagioclase reflects increase in temperature, this would conflict with the P-T estimates from thermobarometry. This inconsistency may be explained by an influx of Ca from an external source via metasomatic reactions between the enclave and its host.

Epidote

Zonation of iron-poor epidote (clinozoisite) at the core, intermediate-iron epidote (zoisite) between the core and rim, and iron-rich epidote (epidote) near the rim of the calc-silicate enclaves may be a response to a change in pressure and/or temperature, metasomatic reactions owing to a change in chemical environment, or a combination of the two via coupled reactions such as Fe^{3+}-poor epidote + andradite = Fe^{3+}-rich epidote + Fe^{3+}-poor phase, such as hornblende or biotite.

Interaction of calc-silicate enclaves with the host felsic magma and pelitic enclaves, which were previously isolated from the calc-silicates, provide a source

for the increase in Ca and Fe. Components are more easily exchanged between the host and the enclaves via metasomatic reactions during entrainment.

5.2 Consistency of P-T Estimates and P-T Path with Petrography

Aluminum silicate polymorphs

Relict sillimanite with minor kyanite in the pelitic enclaves suggests that pre-entrainment metamorphism was near the univariant line for the stability of sillimanite and kyanite (Holdaway, 1971). However, at 5.6 kb, temperatures less than 600 °C are required to stabilize kyanite (Fig. 4.2). At 780 °C, a pressure greater than 9 kb is needed stabilize kyanite. Therefore, temperatures and pressures of 780 °C and 5.6 kb should only produce sillimanite (Fig. 4.2).

Kyanite may have existed metastably in the sillimanite field. However, the pressure and temperature estimates are well within the stability field of sillimanite (Fig. 4.2). However, the calculated pressures may not be the true equilibrium P, as indicated by the aluminum silicates, but rather a minimum estimate.

Abundant fibrolite is consistent with syn-entrainment metamorphism and rapid cooling of the host magma. The lack of andalusite in the enclaves, indicate that syn-entrainment pressures were probably within the upper range of the 2.3 $\pm$ 1.5 kb estimate.

Staurolite and Zincian Hercynite

Staurolite, and zincian hercynite with rims of staurolite, are relict phases in the enclaves. Experiments by Schulters and Bohlen (1989) show that the addition of zinc to hercynite increases the stability field of hercynite to include lower temperature and pressures than for pure hercynite. Temperatures and pressure calculated by Schulters and Bohlen (1989) with spinel-sillimanite-garnet-corundum thermobarometry are as low as 680 °C and 5.5 kb for zinc- rich

hercynite. The temperature and pressure conditions for pre-entrainment metamorphism of the the Ten Mile Lake enclaves (780 ± 50 °C and 5.6 ± 1.5 kb) overlap with the stability of zincian hercynite determined by Schulters and Bohlen (1989).

Staurolite, which re-hydrates below ~ 680 °C and breaks down below ~ 500 °C, may rim zincian hercynite in response to a decrease in temperature. However, spinel is generally associated with silica-poor rock. Schumacher (1985), Stoddard (1979), and Atkin (1978) show that zincian hercynite is produced by the dehydration of staurolite by progressive metamorphism. Thus, staurolite could be produced by the reverse reaction. Petrography shows idioblastic green spinel with inclusions of hematite is rimmed with staurolite containing inclusions of magnetite and quartz, suggesting the reaction

$$sp + bt + Al_2SiO_5 + hem + H_2O \rightleftharpoons st + mus + mt + qz + O_2 .$$

Water may have been introduced by dehydration reactions of in the pelitic enclaves and from the calc-silicate enclaves via microfractures. Carbonate and silica veinlets with Fe-Ti oxides cut the host and pelitic enclaves, consistent with the production of excess silica in the conversion of spinel to staurolite.

5.3 Origin of the Enclaves

In light of the complex zonation of garnet and plagioclase, veinlets, and mineral reactions it appears there has been an increase of Fe, Mn, Ca, and Si in the pelitic rocks. An increase of Fe and Al from the core to the rim of the calc-silicates to the metapelites or host is suggested by the presence of epidote-zonation and aluminum silicate in the calc-silicate.

Thus, comparing the bulk compositions of these enclaves to possible sources, such as the Liscomb gneisses or the Meguma Group, would be difficult

considering the disaggregation of some of the enclaves and the obvious exchange of elements and fluids to and from the pelitic and calc-silicate xenoliths, seen as mineral reactions and veinlets.

The source of the zinc in the some of the pelitic enclaves is unknown, but may be of primary sedimentary origin, or derived from sulfides present in the granite, the source rock, or from the calc-silicate. Zincian hercynite is stable during the higher grade pre-entrainment metamorphism at depths of at least 15 km, therefore it is most probable that zinc was present in the source region of the pelitic enclaves, before their incorporation into the intrusion.

Pre-entrainment pressure estimates and mineralogy indicate that the enclaves are derived from a depth of approximately 17 km and are consistent with amphibolite facies, regional metamorphism.

5.4 Implications on the Liscomb Complex and the Meguma Group

This study shows that in the area of the drill hole, many small enclaves are hosted in a tonalite to quartz-diorite in contact with the Liscomb gneisses. The dimensions of this felsic intrusion is unknown.

The source of the enclaves, as suggested in Figure 5.1, is a pelitic and calc-silicate metasedimentary unit which may represent or underlie the lower Goldenville Formation of the Meguma Group and probably overlay the Liscomb gneisses at a depth of approximately 17 km. The source rock of the pelitic enclaves is locally zinc-rich, as indicated by the presence of zincian hercynite as a pre-entrainment phase.

The intrusion of the magma initiated the diapiric uplift of the gneisses (Giles and Chatterjee 1987a). The enclaves were subsequently included in a tonalite to quartz-diorite intrusion at 2.3 kb or 7 km and equilibrated at approximately 560 °C. The pressures and temperatures obtained for pre- and syn-entrainment

metamorphism of enclaves in this study are similar to the those determined from the study of gabbroic enclaves in the Ten Mile Lake quartz-gabbro to diorite (5.2 $\pm$ 1 kb and 3.3 $\pm$ 1 kb, respectively) (Richard, *manu. in prep.*).

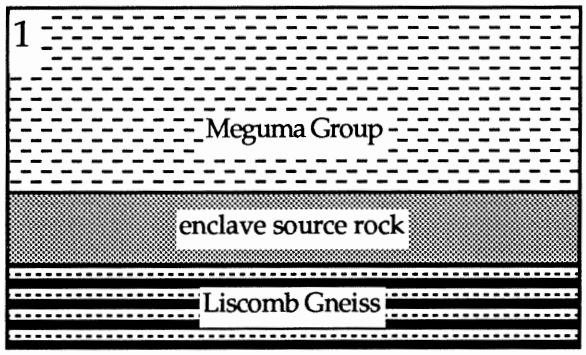

METAMORPHISM 1:

MINERALOGY
garnets G1A and G2A
biotite
zincian hercynite with rims of staurolite
kyanite/sillimanite/fibrolite
plagioclase

P: 5.6 + 1.5 Kb (≈ 17 km)
T: 780 + 50 ° C

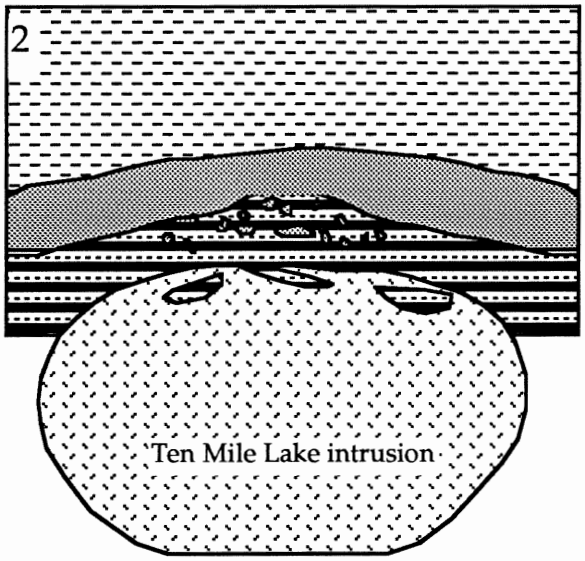

Initial intrustion of the Ten Mile Lake magma leading to the diapiric uplift of the Liscomb gneisses with the incorporation of the metasedimentary enclaves.

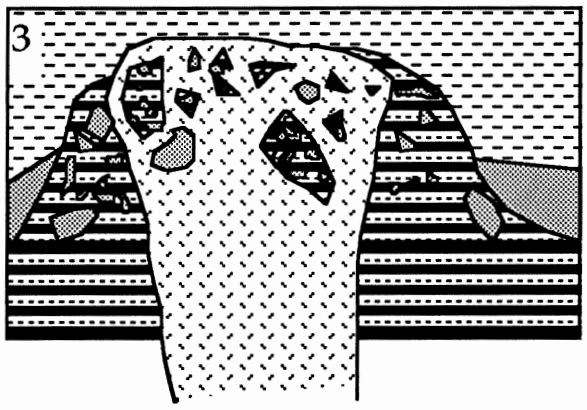

METAMORPHISM 2

MINERALOGY
garnets G1B and G2B
biotite
muscovite
fibrolite
plagioclase

P: 2.3 + 1.5 kb (≈ 7 km)
T: 560 + 50° C

Figure 5.1. History of the Ten Mile Lake enclaves. Pre-entrainment metamorphism at 780 ± 50° C and 5.6 ± 1.5 kb preceded the incorporation of the enclaves into the Liscomb gneisses. The gneisses with the metasedimentary enclaves subsequently become xenoliths in the Ten Mile Lake intrusion at 560 ± 50 ° C and 2.3 ± 1.5 kb.

CHAPTER 6: CONCLUSIONS

Metapelitic and calc-silicate enclaves are hosted in a quartz-diorite to tonalite which is in contact with the Liscomb gneiss, a heterogeneous high-grade rock of igneous and sedimentary origin. The host of the meta-sedimentary enclaves is more felsic than the Ten Mile Lake quartz-normative gabbros and diorites which contain abundant amphibole. Mineralogy of the host rock includes plagioclase, quartz, biotite, muscovite, pyrite, chalcopyrite, and tourm-aline. The enclaves vary from having distinct boundaries to being disaggregated and xenocrystic in the matrix. Petrography, texture, mineral chemistry and zonation, and pressure and temperature estimates have been used to determine the history of these enclaves. Two stages of metamorphism are recognized.

Pre-entrainment pressure and temperature conditions, estimated at 780 $\pm$ 50° C and 5.6 $\pm$ 1.5 kb, are determined from Mn-rich and Mn-poor xenoblastic garnets with inclusions of biotite, quartz, plagioclase, fibrolite, and Fe-Ti oxides and biotite, quartz and Fe-Ti oxides, respectively. The pre-entrainment metamorphism is associated with kyanite, sillimanite, zincian hercynite, staurolite, and complexly zoned plagioclase in the matrix.

Syn-entrainment pressure and temperature conditions of 560 $\pm$ 50° C and 2.3 $\pm$ 1.5 kb are determined from idioblastic Mn-rich garnets with matrix biotite, plagioclase, fibrolite, Fe-Ti oxides, and quartz and idioblastic Mn-poor garnets with inclusion of biotite and Fe-Ti oxides.

The pressure and temperature estimates for these enclaves (780 $\pm$ 50° C and 5.6 $\pm$ 1.5 kb) are at the lower end of the temperature range determined by Chatterjee (750° to 1200° C) (*unpubl. pers. comm*, 1989) for the Liscomb gneisses. The P-T estimates for enclaves examined in this study give pre- and syn-

entrainment pressures indicating shallower depths than the meta-sedimentary and igneous enclaves from the Tangier/Popes Harbour dyke (12-14 kb and greater than 1000°C and 4.5-6 kb and greater than 600° C, respectively).

Bulk chemistry and petrology of the host rock should be obtained in light of the apparent difference in composition from the Ten Mile Lake gabbro. The classification of the host as tonalite to quartz-diorite is based only on rough estimates of mineral content. More detailed work must be done to better classify the intrusion. The dimensions of the intrusion should be determined by mapping, drilling, and geophysical techniques.

The limited number of samples and even more limited number suitable for P-T estimates means that further investigation is needed to either confirm or disprove the conclusions of this study. Pressures determined from mafic enclaves (5.2 $\pm$ 1 kb) and their host, the Ten Mile Lake gabbro (3.3 $\pm$ 1 kb) (Richard, *manu. in prep*) are similar to those of this study. This might indicate a heterogeneous crust at 5 kb or show that this is the transition from the lower Meguma Group to the Liscomb gneisses at depth. More sampling may provide enclaves from different levels in the lower crust to provide a profile of lithologies, grades of metamorphism, and an answer to the question of a possible heterogeneity or transition of the of the crust at 5.4 kb.

Syn-entrainment pressure estimates for both studies indicate a depth of approximately 12 km for both the felsic and mafic intrusions in the Ten Mile Lake area.

Ages may be determined for the pre- and syn-entrainment metamorphism using inclusions of biotite in relict garnets and matrix biotite, respectively. The age of the felsic intrusion which hosts the enclaves examined in this study should be determined and compared to its neighbouring mafic intrusion.

ACKNOWLEDGEMENTS

I wish to thank A Chatterjee for discussions pertaining to the Liscomb Complex, R MacKay for his demonstration of the microprobe, M Haggart for many informative discussions on thermobarometry, and DB Clarke and L Richard for discussions, preprints, and many useful suggestions. Thanks is also extended to R Hasen, who unselfishly made available her Macintosh computer and her time to teach me the wonders of computer graphics, and to R Hicks and D Ritcey for their much appreciated help during this study and preparation of the thesis. Special thanks are extended to RA Jamieson for her guidance and support throughout the course of this study.

REFERENCES

Atkin BP (1978) Hercynite as a breakdown product of staurolite within the aureole of the Ardara Pluton. Co. Donegal, Eire. Mineralogical Magazine 42 :237-239.

Carmichael DM (1969) On the mechanism of prograde metamorphic reactions in quartz-bearing pelitic rocks. Contributions to Mineralogy and Petrology 20: 244-267.

Chatterjee AK and Giles PS (1988) Al-rich pyroxenes in granulite xenoliths from Tangier: implications to lower crustal continental crust, eastern Meguma zone. In: Mines and Mineral Branch, Report of Activities 1987, Part B; Nova Scotia Department of Mines and Energy, Report 88-1: 248-249.

Douma SL (1988) Preliminary report on the metamorphic history of Meguma Group metasediments in eastern Nova Scotia: regional and contact metamorphism. In: Mines and Mineral Branch, Report of Activities 1987, Part B; Nova Scotia Department of Mines and Energy, Report 88-1: 121-127.

Eberz GW, Clarke DB, Chatterjee AK, and Giles PS (1989) The chemical and Isotopic composition of the lower crust beneath the Meguma zone, Nova Scotia: Evidence from lower crustal xenoliths. Submitted to Geochimica et Cosmochimica Acta.

Eberz GW, Clarke DB, Chatterjee AK, and Giles PS (1988) Geochemistry of the lower crust beneath the Meguma zone, Nova Scotia. In: Mines and Mineral Branch, Report of Activities 1987, Part B; Nova Scotia Department of Mines and Energy, Report 88-1: 251-252.

Essene EJ (1989) The current status of thermobarometry in metamorphic rocks. In: Evolution of Metamorphic Belts Daly JS, Cliff, RA, and Yardley, BWD (eds) Geological Society Special Publication 43: 1-44.

Faribault ER (1901,1902) Geological Map of Nova Scotia, Halifax and Guysborough Counties.

Ferry JM and Spear FS (1978) Experimental calibration of partitioning of Fe and Mg between biotite and garnet. Contributions to Mineralogy and Petrology 66: 113-117.

Ganguly J and Saxena SK (1984) Mixing properties of aluminum silicate garnets: constraints from natural and experimental data, and applications to geothermo-barometry. American Mineralogist 69: 88-97.

Ghent ED, Robbins DB, and Stout MZ (1979) Geothermometry, geobarometry, and fluid fluid compositions of metamorphosed calc-silicates and pelites, Mica Creek, British Columbia. American Mineralogist 64: 874-885.

Giles PS and Chatterjee AK (1987a) Evolution of the Liscomb Complex and relevance to metallogeny in the eastern Meguma zone. In: Mines and Mineral Branch, Report of Activities 1986; Nova Scotia Department of Mines and Energy, Report 87-1: 191.

Giles PS and Chatterjee AK (1987b) Lower crustal xenocrysts in xenoliths in the Tangier Dyke, in the eastern Meguma zone. In: Mines and Mineral Branch, Report of Activities 1987, Part A; Nova Scotia Department of Mines and Energy, Report 87-5: 85-88.

Giles PS and Chatterjee AK (1986) Peraluminous granites of the Liscomb Complex; In: Tenth Annual Open House and Review of Activities Programs and summaries. Nova Scotia Department of Mines and Energy, Information Series 12: 83-89.

Hodges KV and Crowley P (1985) Errors estimation and empirical geothermobarometry for pelitic systems. American Mineralogist 70: 702-709.

Holdaway MJ (1971) Stability of andalusite and the aluminum silicate phase diagram. American Journal of Science 271: 97-131.

Indares A and Martignole J (1985) Biotite-garnet geothermometry in granulite phases: the influence of Ti and Al in biotite. American Mineralogist 73: 216-223.

Keppie JD and Muecke GK (1979) Metamorphic Map of Nova Scotia, In: Geological Map of the Province of Nova Scotia, compiled by JD Keppie, Nova Scotia Department of Mines and Energy, published map scale 1: 1 000 000.

Kerrick DM (1987) Fibrolite in contact aureoles of Donegel, Ireland American Mineralogist 72: 240-254.

Nadeau L. PTLEO. Computer software. University of Ottawa. unpublished.

Newton RC and Haselton HT (1981) Thermodynamics of the garnet - plagioclase - Al_2SiO_5 - quartz geobarometer. In: Thermodynamics of Mineral and Melts. Advances in Physical Geochemistry v. 1. Newton RC, Navrotsky, A and Wood, BJ (eds) Springer-Verlag, New York, p. 131-147.

Owen JV, Greenough JD, Hy, C, and Ruffman A (1988) Xenoliths in a mafic dyke at Popes Harbor, Nova Scotia: implication for basement to the Meguma Group. Canadian Journal of Earth Science 25: 1464-1471.

Schulters JC and Bohlen SR (1989) The stability of hercynite and hercynite-gahnite spinels in corundum- or quartz bearing assemblages. Journal of Petrology 30: 1017-1031.

Schumacher R (1985) Zincian staurolite in Glen Doll, Scotland. Mineralogical Magazine 49: 561-571.

Stoddard EF (1979) Zinc-rich hercynite in high-grade metamorphic rocks.: a product of the dehydration of staurolite. American Mineralogist 64: 736-741.

Thompson AB (1976) Mineral reactions in pelitic rocks: II calculations of some P-T-X (Fe-Mg) Phase relations. American Journal of Science 276: 425-454.

Yardley, BWD (1989) An introduction to metamorphic petrology. Longman Earth Science Series, New York, pp. 248.

Yardley, BWM (1981) A note on the composition and stability of Fe-staurolite. Nueus Jahrbuch fur Mineralogie Monatschafte Jg. 1981: 127-132.

APPENDIX I
MINERAL TABLE

All sections contain quartz, plagioclase, muscovite, sphene, pyrite, chalcopyrite, Fe-Ti oxides, and retrograde chlorite.

	brown biotite	tourmaline	fibrolite	sillimanite (relict)	kyanite (relict)	staurolite (relict)	garnet (late)	garnet (early)	grossular	apatite	spinel (relict)	hornblende	zoisite	clinozoisite	epidote	dolomite
1A									x			x				x
1B	x		x			x	x	x				x	x		x	
1C	x		x	x	x		x	x								
2A	x		x			x	x	x				x				
2B	x		x	x		x	x	x								
2C	x		x				x	x				x				
3A	x		x	x		x	x	x								
3B	x		x	x	x	x	x	x								
4A	x	x	x				x	x								
4B	x		x				x	x								
5A	x		x			x	x	x								
5C	x		x					x	x							
5D	x		x				x	x			x	x				
6A	x		x						x	x		x				x
6B	x		x	x		x										
6C	x		x	x			x	x			x					
6D	x		x				x	x								
7A	x	x	x			x	x	x			x					
7B	x		x			x	x	x								
7C	x		x				x									
8A	x	x	x	x			x	x			x	x				
8B	x	x	x	x	x		x	x								
8C	x		x			x	x	x			x	x				
8D	x		x					x	x		x	x	x	x	x	x

APPENDIX II
THIN SECTION DESCRIPTIONS

TML-1A

Calc-silicate. Xenoblastic carbonate, epidote, minor grossular, and sphene (less than 0.25 mm xenoblastic, idioblastic 0.1 mm) clusters in quartz and lesser plagioclase matrix. Carbonate is enclosed in epidote and actinolite. Hornblende is partially chloritized and associated with the sulfides. Chlorite also after garnet. Plagioclase (less than 1 mm), a minor common of this calc-silicate, is associated with sericite and less often muscovite.

TML-1B

Pelite and calc-silicate in an igneous host. Minor calc- silicate regionof predominantly epidote, quartz, and hornblende has undergone extensive fibrolitization of muscovite, biotite, and plagioclase is reacting to produce fibrolite. Much of the biotite is resorbed and highly embayed and is associated with plagioclase, opaques, and quartz suggests the break down of biotite to opaques, fibrolite and sericite. Retrograde chlorite after biotite evident.Relict garnet has also under gone extensive resorption. Replacement of of plagioclase by muscovite hosting fibrolite.

TML-1C

Pelite. Similar to 1B with extensive replacement of muscovite and biotite by fibrolite. The biotite is small xenoblastic showing evidence for resorption. Sericitization of plagioclase very common particularly in area adjacent to areas of the most intense fibrolitization. Chlorite after biotite. Minor kyanite is rimmed with fine muscovite. Pyrite with minor chalcopyrite.

TML-2A

Pelite. Embayed biotite, broken down to fibrolite + Fe-Ti oxides forms clusters with seritized plagioclase. Pyrite with minor chalcopyrite, up to 10 mm, are rimmed with biotite. Minor hornblende with a core of brown. Rare staurolite is highly resorbed within muscovite.

TML-2B

Pelite. Ghost mafic enclave with in the xenolith contains coarse randomly orientated biotite with minor relict biotite and retrograde chlorite. Mn-poor relict garnets common in less mafic region. Region 15 mm of radiating retrograde chlorite. plagioclase is replaced by muscovite and fibrolite.

TML-2C

Pelite. Quartz and plagioclase very common with only scare garnet. Embayed biotite associated with retrograde chlorite. Localized sericitization of plagioclase common near clusters of fibrolite pseudomorphs of muscovite. A large igneous plagioclase xenocryst in matrix.

TML-3A

Pelite. Several small enclaves. Pyrite-rich with minor chalcopyrite are rimmed with biotite and subsequently quartz and sericitized plagioclase. Relict garnet, particularly G2 is more common in this region. A dark layer consists of G3 and biotite with garnet less common near the rim of the layer. Biotite is more resorbed outside this zone with quartz and plagioclase dominating. Plagioclase at the near the rim to the garnet and biotite region of more intensely alter to sericite. Relict acicular sillimanite has an alteration rim of sericite.

TML-3B

Pelite. Pyrite with minor chalcopyrite associated with slightly embayed biotite and G3. Muscovite shows replacement to fibrolite. Extremely resorbed biotite, Fe-Ti oxides, and seritized which decreases away from the this region. Relict kyanite and sillimanite with reaction rims are common and best preserved in this section. Relict xenoblastic staurolite (less than 0.2 mm) exhibits a diffusion halo and is included in secondary muscovite. Chess board plagioclase is common. Minor relict garnet is resorbed.

TML-4A

Pelite. Pyrite with minor chalcopyrite band (30 mm) is surrounded by highly resorbed biotite among sub-idioblastic secondary biotite. Minor oumaline rims biotite. Plagioclase (2-3 mm) exhibits complex zoning with an internal rim of sericite between the rim and core. Localized areas of muscovite overgrowths of fibrolite. Garnet is entirely surrounded by plagioclase.

TML-4B

Pelite. A veinlet of quartz is sub-parallel to the contact between the enclave and the host causing seritization of plagioclase in its vicinity. The host is predominantly quartz and plagioclase with Fe-Ti oxides, slightly resorbed Mn-rich garnet, and muscovite and biotite breaking down to form fibrolite. Biotite is resorbed to slightly embayed. Minor fibrolite is present

along plagioclase-plagioclase boundaries. Plagioclase ranges from xenoblastic poly-twinned to sub-idioblastic and idioblastic poly-twinned, albite twined, oscillatory zoned, chess board twins, and exsolution lamellae are present. These are complexly zoned, up to 2-3 mm, and may or may not have seritized cores and anhedral untwinned rims.

TML-5A

Pelite. Zones of intense fibrolitization of muscovite and biotite with associated opaques very common. Biotite is embayed as fibrolite overgrows muscovite. Xenoblastic plagioclase are generally less than 0.5 mm and relict plagioclase may reach 4mm with anhedral rims. Seritization of plagioclase common, especially at the cores of relict plagioclase. Mostly the host granite.

TML-5C

Pelite. Regions of quartz, sulfides, biotite, tourmaline and plagioclase + chlorite. The quartz region contains large xenoblastic crystals (1mm) of quartz. Other minerals are absent. Pyrite is embayed and trap quartz with inclusions of idioblastic biotite, apatite, and muscovite (0.01 mm). The biotite region is dense cluster (3-4 cm) of predominantly resorbed biotite with opaques and quartz. The area of plagioclase and chlorite intergrowth is 25 mm. Plagioclase (5-6 mm) are poly-twinned with muscove growth and sericitic alteration. These are rimmed with anhedral plagioclase which lack twinning and exsolution. Remainder of xenolith is typically biotite and muscovite are pseudomorphed by fibrolite and opaques in a quartz and plagioclase.

TML-5D

Pelite. Quartz and plagioclase common. Plagioclase are xenoblastic (0.25mm) and sub-idioblastic (1-2mm) with chess board textures, untwinned rims and seritization common particularly near areas of localized intense fibrolitization. Fibrolite is observed to surround and pseudomorph biotite and to a lesser degree muscovite. Relict garnet is highly fractured and broken.

TML-6A

Calc-silicate with pelite. The calc-silicate minerals are enclosd in coarse quartz. Calc-silicate minerals grow between quartz grains and along fractures to the pelite. Veinlets of epidote and rare amphibole penetrate through quartz and calc-silicate minerals perpendicular to the pelite interface and generally diffuse minerals parallel along it. There is a distinct grain size difference in the quartz in the calc-silicate (3-5 mm) and quartz of the host (1 mm). Xenoblastic grossular with inclusions of carbonate is common at the core.

Clinozoisite, garnet, and zoisite. Epidote is most predominant along veins. The Pelite portion of the xenolith is characterized by localized extensive fibrolitization and opaques. Chessboard plagioclase and sericitic alteration is common particularly in areas surrounding fibrolite.

TML-6B

Pelite. A 15 mm light band consists of fibrolite to acicular sillimanite after biotite and muscovite with chessboard and poly-twinned plagioclase with seritized core and resorbed biotite. It is separated from a region of extensive seritization of plagioclase, quartz and minor biotite by a 2-3 mm biotite rich band on either side. The biotite is slightly embayed to sub-idioblastic with Fe-Ti oxides, plagioclase, and quartz.

TML-6C

Pelite. Idioblastic biotite (1.5 mm in length) becomes embayed and resorbed near fibrolite. Secondary muscovite (2 mm in length) is slightly embayed near the rim, contains inclusions of biotite, and shows no fibrolitization. Muscovite begins to become more embayed near patches of fibrolite. Relict garnet is corroded and sillimanite is surrounded by quartz. Green spinel (0.2 mm) is close to relict sillimanite and garnet. Sericitization of plagioclase is very common.

TML-6D

Pelite. Fibrolite + pyrite with minor chalcopyrite layer (15 mm) consists of parallel sulfide stringers (1 mm x10 mm). Coarse fibrolite pseudomorphs of biotite are aligned parallel to the sulfides. Relict garnet is corroded. Chessboard twins and xenoblastic plagioclase common with minor replacement by myrmekite intergrowth of plagioclase and quartz. Sericitization occurs between the rim and core of the plagioclase. Late pseudomorphs of muscovite by fibrolite are present. The sillimanite poor- layers contain more biotite, with quartz, plagioclase, Fe-Ti oxides, and muscovite.

TML-7A

Pelite. Angular to slightly rounded zone (less than 10 mm) rich in resorbed biotite, quartz, opaques, and idioblastic to sub-idioblastic muscovite. Relict green spinel in muscovite. Plagioclase is xenoblastic (0.25 mm) to sub-idioblastic with anhedral rims (1mm) or has chessboard twins. Patch of fibrolite with inclusion of biotite and staurolite which is rimmed with quartz. Fibrolite is pseudomorphing biotite with Fe-Ti oxides. Relict garnets are

highly corroded. Secondary idioblastic biotite and muscovite up to 1mm in length.

TML-7B

Pelite. Biotite band (5 mm) is asymmetrically kinked. This biotite is resorbed and fibrolitized with opaques,quartz, plagioclase, and chlorite. Relict staurolite has inclusions and is rimmed with biotite and is included in secondary idioblastic muscovite. Pseudomorphs of fibrolite after biotite are surrounded by resorbed biotite and secondary muscovite and biotite. The light layer contains less biotite and is predominantly quartz with sericitized plagioclase,biotite, opaques, and muscovite. The plagioclase are xenoblastic and poly-twinned, with or without chessboard twinning and anhedral rims.

TML-7C

Pelite. Localized clusters of fibrolite and Fe-Ti oxides. Predominantly quartz and seritized plagioclase, idioblastic biotite and muscovite. Also , slightly embayed biotite to highly mottled. Anhedral plagioclase and anhedral rims on idioblastic relict plagioclase. Muscovite shows overprinting of fibrolite with minor opaques.

TML-8A

Pelite. A distinct slightly angular to rounded enclave is a dense cluster of garnet and biotite which is in sharp contact with the host. Large plagioclase (4 mm x 2 mm) fractured, twinned and is rimmed with anhedral plagioclase. The matrix contains relict sillimanite with sericite rims and slightly embayed biotite. Tourmaline is associated with pyrite.

TML-8B

Pelite. Angular region (15 x 10 mm) of biotite, plagioclase, quartz, and Fe-Ti oxides has a distinct area in which the assemblage rapidly becomes less mafic. Also a quartz rich host with apatite and a region sericitized plagioclase. A sulfide vein rimmed with green biotite and opaques cut the xenolith. Sericitization in the vicinity if the vein is extreme and gradual dies away from it. Relict sillimanite after biotite is preserve 0.1 mm away from late cluster of fibrolite. An area rich in relict minerals contains several garnets with quartz, biotite, fibrolite, plagioclase inclusions, resorbed biotite, and minor green spinel rimmed with staurolite.

TML-8C

Veinlet (0.25 mm) of carbonate with minor opaques rimmed with tourmaline cuts through the xenolith. An distinct angular cluster (10 x 25 mm) of late Mn-rich + idioblastic biotite biotite + plagioclase + quartz is rimmed by sericitized plagioclase. Relict sub-idioblastic staurolite with inclusions of quartz is preserved. Minor zincian hercynite (0.1mm) with inclusions of hematite and enclosed in staurolite is included in biotite. Acicular sillimanite anhedral biotite + chlorite + Fe-Ti oxides + staurolite. Plagioclase is anhedral or idioblastic with seritized cores and anhedral rims.

TML-8D

Pelite enclave with 2 cm calc-silicate nodule in a igneous host. The calc-silicate nodule is zoned from the core from the rim containing an array of calc-silicate minerals embayed in a quartz matrix which becomes less important to the rim near the pelite. The core is carbonate + clinozoisite + grossular grading into epidote + clinozoisite + zoisite, epidote and finally epidote + hornblende + biotite. Veinlets (0.1 mm) of carbonate + quartz reach into the core of the calc-silicate and finally dissipate in the pelite. The pelite section contains anhedral, chessboard, wormy, and oscillatory zoned plagioclase with anhedral rims of plagioclase. Localized areas of anhedral biotite with opaques and acicular sillimanite. Relict garnet show extensive resorption. Relict green sub-idioblastic zincian hercynite (0.1 mm) with inclusions of hematite is rimmed with clear to light yellow staurolite with magnetite inclusions. Quartz inclusions are concentrated along the spinel - staurolite boundary. The staurolite with spinel core reach up to 0.25 mm.